CCL2-CCR2 signaling in the skin drives surfactant-induced irritant contact dermatitis via IL-1β-mediated neutrophil accumulation

Rintaro Shibuya MD[a], Yoshihiro Ishida MD, PhD[a], Sho Hanakawa PhD[b], Tatsuki R Kataoka MD, PhD[c], Yasuhide Takeuchi MD, PhD[d], Teruasa Murata MD, PhD[a], Arisa Akagi MD[a], Zachary Chow PhD[b], Toshiaki Kogame MD, PhD[a], Satoshi Nakamizo MD, PhD[a], Saeko Nakajima MD, PhD[a], Gyohei Egawa MD, PhD[a], Takashi Nomura MD, PhD[a], Naotomo Kambe MD, PhD[a], Akihiko Kitoh MD, PhD[a, b], and Kenji Kabashima MD, PhD[a,b]

[a] Department of Dermatology, Kyoto University Graduate School of Medicine, Japan

[b] Singapore Immunology Network and Skin Research Institute of Singapore, Agency for Science, Technology and Research (A*STAR), Singapore

[c] Department of Molecular Diagnostic Pathology, Iwate Medical University, Japan

[d]Department of Diagnostic Pathology, Kyoto University Graduate School of Medicine, Japan

Correspondence should be addressed to Akihiko Kitoh, MD, PhD

Department of Dermatology, Kyoto University Graduate School of Medicine

54 Shogoin Kawara, Sakyo-ku, Kyoto 606-8507, Japan

Tel: +81-75-751-3310

Fax: +81-75-751-4949

E-mail: kichu@kuhp.kyoto-u.ac.jp (AK)

Abstract

Surfactant-induced cumulative irritant contact dermatitis (ICD) is a common and clinically important skin disorder. CCL2 is known to mediate inflammation following tissue damage in various organs. Thus, we investigated whether and how CCL2 contributes to the development of murine cumulative ICD induced by a common surfactant, sodium dodecyl sulfate (SDS). Wild-type mice treated topically with SDS for 6 consecutive days developed skin inflammation that recapitulated the features of human cumulative ICD, including barrier disruption, epidermal thickening, and neutrophil accumulation. CCL2 was upregulated in SDS-treated skin, and local CCL2 blockade attenuated SDS-induced ICD. SDS-induced ICD and neutrophil accumulation were also attenuated in mice deficient in CCR2, the receptor for CCL2. Neutrophil depletion alleviated SDS-induced ICD, suggesting that impaired neutrophil accumulation was responsible for the amelioration of ICD in CCR2-deficient mice. In RNA-seq analyses of SDS-treated skin, the expression levels of *Il1b* in CCR2-deficient mice were highly downregulated compared with those in wild-type mice. Furthermore, the intradermal administration of IL-1β in the SDS-treated skin of CCR2-deficient mice restored the local accumulation of neutrophils and the development of ICD. Collectively, our results suggest that CCL2-CCR2 signaling in the skin critically promotes the development of SDS-induced ICD by inducing IL-1β expression for neutrophil accumulation.

Abbreviations

Ab, Antibody

BM, Bone marrow

CCL, CC chemokine ligand

CCR, CC chemokine receptor

IL, Interleukin

PBS, Phosphate buffered saline

SDS, Sodium dodecyl sulfate

TNF, Tumor necrosis factor

WT, Wild-type

Short Title: CCL2 in the skin drives irritant contact dermatitis

INTRODUCTION

Irritant contact dermatitis (ICD) is a common skin disorder caused by exposure to chemicals with irritant properties (Gittler et al. 2013). ICD can develop after a single overwhelming exposure to an irritant (acute ICD); however, it is often caused by multiple subthreshold insults induced by weak irritants, such as surfactants contained in soaps, shampoos, and detergents (cumulative ICD) (Slodownik et al. 2008). This disorder is characterized by skin inflammation and skin barrier disruption with immune cell infiltration and, in the case of the cumulative type, epidermal hyperplasia (Cohen, E. 2018). ICD is the most common form of occupational skin disorder and leads to an impaired quality of life and reduced productivity (Dickel et al. 2002; Dietz et al. 2020). In addition, exposure to irritants could be involved in both the development and aggravation of atopic dermatitis (Akdis et al. 2006; Williams et al. 2007). Thus, it is essential to manage ICD based on an understanding of its pathogenesis.

The release of soluble mediators from skin cells (principally keratinocytes) damaged by irritants induces an inflammatory cytokine/chemokine milieu with immune cell accumulation, leading to the development of ICD (Gittler et al. 2013; Slodownik et al. 2008). However, the roles of only limited cytokines (TNF-α, IL-6, and IL-10) in ICD have been evaluated *in vivo* (Berg et al. 1995; Lee et al. 2013; Piguet 1991). As for immune cells, accumulation of neutrophils and lymphocytes in the lesional skin of human ICD has been described, although patterns of immune cell infiltration have not been well investigated (Weedon 2010). In murine ICD, local

accumulation of various types of immune cells, including neutrophils, monocytes, eosinophils, basophils, and lymphocytes, has been reported (Anderson et al. 1986; Calhoun et al. 2019). Previous *in vivo* studies, including ours, have suggested that eosinophils, basophils, and $CD4^+$ cells contribute to the development of croton oil-induced acute ICD (Kondo et al. 1996; Nakashima et al. 2014). However, the roles of neutrophils and monocytes in the pathogenesis of murine ICD remain unclear, although they are the major cell subsets infiltrating the lesional skin. In addition, which cytokine/chemokine critically controls the local accumulation of immune cells responsible for the development of ICD also remains to be elucidated.

Among many proinflammatory cytokines/chemokines, CC chemokine ligand (CCL) 2 has been implicated as an important mediator of inflammation following sterile insults to organs, such as ischemia-induced damage in the brain, liver, and kidney (Dimitrijevic et al. 2007; Kashyap et al. 2018; Zhang et al. 2016). CCL2 exerts its chemotactic function via CC chemokine receptor (CCR) 2 expressed on hematopoietic cells, such as monocytes and certain types of progenitor cells (Andres et al. 2011; Ishida et al. 2019; Willenborg et al. 2012). In the skin, CCL2 promotes wound healing (Ishida et al. 2019) and skin fibrosis (Arai et al. 2013) by attracting immune cells, in particular monocytes. However, the role of CCL2 in the pathogenesis of ICD has not been evaluated *in vivo*, although the chemokine is upregulated in surfactant-irritated murine and human skin (Lee et al. 2013; Meller et al. 2007).

In this study, we evaluated the role of CCL2 in the development of surfactant-induced cumulative ICD in mice. We revealed that CCL2 in the skin is

essential for the development of murine ICD following repeated exposure to a surfactant, sodium dodecyl sulfate (SDS). The development of SDS-induced ICD was dependent on CCR2 expression in the radioresistant compartment of the skin. Furthermore, neutrophils were responsible for the induction of SDS-induced ICD and their accumulation in lesions was mediated by CCR2-dependent IL-1β production.

RESULTS

Repeated topical application of SDS-induced cumulative ICD in mice

We first established a murine model of cumulative ICD induced by repeated exposure to surfactant SDS, one of the most common causative agents of human ICD. Ear skin of wild-type (WT) mice was treated topically with SDS or phosphate-buffered saline (PBS) for 6 consecutive days. The repeated topical application of SDS induced skin inflammation characterized by skin roughness and mild erythema with significant ear swelling, while PBS-treated skin showed no observable signs of inflammation (Figure 1a and b). In addition, SDS-treated skin showed a marked increase in transepidermal water loss (TEWL) on day 6, indicating skin barrier disruption (Figure 1c). Histological analysis revealed significantly greater epidermal thickness and dermal infiltration of immune cells in SDS-treated skin than in PBS-treated skin (Figure 1d and e). These phenotypic and histological findings were consistent with the previously reported features of cumulative ICD in humans (Slodownik et al. 2008). In addition, histological examination of a biopsy specimen taken from an individual with human cumulative ICD revealed epidermal thickening and the dermal infiltration of immune

cells (Figure 1f). Flow cytometric analysis revealed marked infiltration of neutrophils in the lesional skin (Figure 1g and Supplementary Figure S1), as reported in human ICD (Weedon 2010). Other innate immune cells such as monocytes, eosinophils, basophils, and macrophages also accumulated in the SDS-treated skin, while numbers of both αβ and γδ T cell subsets were not increased by SDS treatment (Figure 1g and Supplementary Figure S1). Collectively, we established a murine model of cumulative ICD induced by surfactant SDS.

Locally produced CCL2 was required for the development of SDS-induced ICD

We hypothesized that CCL2 is produced in SDS-irritated skin, critically contributing to the development of ICD. To verify this hypothesis, we first evaluated the mRNA expression levels of *Ccl2* in SDS-treated skin at different time points (days 0, 2, 4, and 6) by quantitative reverse transcription polymerase chain reaction. *Ccl2* expression was significantly upregulated on day 4 compared to day 0 (Figure 2a). In addition, an enzyme-linked immunosorbent assay showed that CCL2 protein levels were significantly higher in SDS-treated skin than in PBS-treated skin on day 6 (Figure 2b). To identify the cell sources of CCL2 in SDS-treated skin, we performed RNA *in-situ* hybridization of *Ccl2* in combination with immunofluorescence staining for vimentin (a marker for mesenchymal cells) or CD45 (a marker for hematopoietic cells). More *Ccl2*-expressing cells were detected in SDS-treated skin on day 4 than on day 0 (Figure 2c). Many of *Ccl2*-positive cells were positive for vimentin, while few *Ccl*2-positive cells expressed CD45 (Figure 2c and Supplementary Figure S2). Moreover, a

substantial number of cells expressing *CCL2* mRNA were detected in lesional skin of human cumulative ICD but not in normal control skin (Figure 2d). In addition, *CCL2*/vimentin double-positive cells were detected (Figure 2d). Thus, in both mice and humans, CCL2 is likely to be produced in the lesional skin of cumulative ICD, at least in part by mesenchymal cells.

To evaluate the role of CCL2 in the pathogenesis of SDS-induced ICD, we generated CCL2-deficient mice by crossing $Ccl2^{fl/fl}$ mice with $E2a^{Cre}$ mice, which mediates ubiquitous deletion of *loxP*-flanked *Ccl2* gene segments (denoted as $Ccl2^{fl/fl}E2a^{Cre}$ mice). We observed less ear swelling after repeated SDS application in $Ccl2^{fl/fl}E2a^{Cre}$ mice than in control $Ccl2^{fl/fl}$ mice (Figure 2e). In addition, SDS-induced epidermal thickening and increased TEWL were significantly lower in $Ccl2^{fl/fl}E2a^{Cre}$ mice than in $Ccl2^{fl/fl}$ mice (Figure 2f and g). Flow cytometric analysis revealed that levels of neutrophil, monocyte, and eosinophil accumulation in SDS-treated skin were significantly lower in $Ccl2^{fl/fl}E2a^{Cre}$ mice than in $Ccl2^{fl/fl}$ mice (Figure 2h). By contrast, the accumulation of basophils was comparable in these two groups (Supplementary Figure S3), suggesting that basophils are not involved in the mechanisms by which CCL2 promotes the development of SDS-induced ICD.

Next, we examined whether the neutralization of CCL2 in the SDS-treated skin inhibits disease development. Ears treated intradermally with an anti-CCL2 antibody (Ab) exhibited milder SDS-induced swelling than that of isotype control Ab-treated ears (Figure 2i). This attenuation of ear swelling was accompanied by the impaired accumulation of neutrophils, monocytes, and eosinophils in the SDS-treated skin

(Figure 2j). These results suggest that locally produced CCL2 plays an important role in the development of SDS-induced ICD.

CCR2 deficiency ameliorated SDS-induced ICD

The major receptor for CCL2 is CCR2 (Andres et al. 2011; Willenborg et al. 2012). Thus, we examined whether the development of SDS-induced ICD was impaired in CCR2-deficient (*Ccr2*$^{-/-}$) mice. *Ccr2*$^{-/-}$ mice exhibited significantly milder ear swelling and epidermal thickening with lower TEWL values on day 6 in comparison with WT mice (Figure 3a-c). Counts of neutrophils, monocytes, and eosinophils in SDS-treated skin were significantly lower in *Ccr2*$^{-/-}$ mice than in WT mice (Figure 3d). Notably, monocyte accumulation in SDS-treated skin was completely abolished in *Ccr2*$^{-/-}$ mice, consistent with a previous finding that the recruitment of monocytes to inflamed tissues depends on their CCR2 expression (Willenborg et al. 2012). Taken together, these results suggest that the CCL2-CCR2 pathway plays an essential role in the development of SDS-induced ICD.

CCR2 deficiency in radiosensitive hematopoietic cells, including monocytes, did not affect the development of SDS-induced ICD

Next, we aimed to determine the CCR2^{+} target cells on which CCL2 acts to drive the development of SDS-induced ICD. CCL2 is a potent chemokine for a variety of CCR2^{+} hematopoietic cells, particularly monocytes (Kurihara et al. 1997; Talbot et al. 2015; Terwey et al. 2005; Tsou et al. 2007). In fact, the amelioration of SDS-induced

ICD by a deficiency in either CCL2 or CCR2 was accompanied by the impaired accumulation of monocytes in the SDS-treated skin, as shown in Figure 2g and 3d. Thus, we hypothesized that CCL2 promoted the development of SDS-induced ICD by promoting the recruitment of monocytes to the lesional skin. To evaluate this hypothesis, we examined the consequences of CCR2 deficiency in hematopoietic cells using a bone marrow (BM) chimera approach. Lethally irradiated WT mice were transplanted with WT or *Ccr2*$^{-/-}$ BM cells and then treated with SDS to induce ICD 12 weeks after transplantation (Figure 3e). The cutaneous accumulation of neutrophils and eosinophils after SDS application was comparable in WT mice reconstituted with WT BM cells and those reconstituted with *Ccr2*$^{-/-}$ BM cells (Figure 3f). By contrast, monocyte accumulation was completely abrogated in *Ccr2*$^{-/-}$ BM-transplanted mice (Figure 3f). However, SDS-induced ear swelling as well as epidermal thickening and increased TEWL were comparable between WT BM- and *Ccr2*$^{-/-}$ BM-transplanted mice (Figure 3g-i). These results suggest that the CCR2-dependent chemoattraction of radiosensitive hematopoietic cells including monocytes into the SDS-treated skin is not required for the development of ICD.

CCR2 signaling in the radioresistant compartment of the skin was required for the development of SDS-induced ICD

Next, we investigated whether CCR2 deficiency in radioresistant cells affects the development of SDS-induced ICD. The SDS-induced ear swelling, epidermal thickening, and increased TEWL were significantly attenuated in *Ccr2*$^{-/-}$ mice

reconstituted with WT BM cells compared to WT mice reconstituted with WT BM cells (Figure 4a-d). The numbers of neutrophils, monocytes, and eosinophils in the SDS-treated skin were significantly lower in *Ccr2*$^{-/-}$ mice reconstituted with WT BM cells than in their WT counterparts (Figure 4e). The attenuated accumulation of these cell subsets was not due to decreases in the peripheral blood, as evidenced by comparable cell counts in the peripheral blood of the two chimera groups (Supplementary Figure S4). These results suggest that CCR2 signaling in radioresistant cells is required for immune cell accumulation in SDS-treated skin and the development of ICD.

CCL2 produced in the skin can act on radioresistant cells both in the skin and in the circulation. Thus, we next asked whether CCR2 in the skin-resident compartment was involved in the development of SDS-induced ICD. To this end, we performed parabiosis experiments in which WT (CD45.1^{+}) and *Ccr2*$^{-/-}$ (CD45.2^{+}) mice were surgically joined to share blood circulation (Figure 4f). After 2 weeks of parabiosis, we confirmed that CD45^{+} cells in the peripheral blood were composed of about 50% CD45.1^{+} (WT-derived) and about 50% CD45.2^{+} (*Ccr2*$^{-/-}$-derived) cells in both WT and *Ccr2*$^{-/-}$ parabionts (Supplementary Figure S5), demonstrating the successful sharing of blood circulation between the parabiont pairs. We then treated both WT and *Ccr2*$^{-/-}$ parabionts with SDS to induce ICD (Figure 4f). SDS-induced ear swelling and the accumulation of neutrophils and monocytes in the skin were significantly attenuated in *Ccr2*$^{-/-}$ parabionts compared to WT parabionts (Figure 4g and h), suggesting that CCR2 in the skin-resident compartment was required for the development of SDS-induced

ICD. Taken together, it is likely that CCR2 signaling in the radioresistant compartment of the skin is essential for inducing innate immune cell accumulation in SDS-treated skin and the development of ICD.

Neutrophil deficiency resulted in the amelioration of SDS-induced ICD

Our results showed that the amelioration of SDS-induced ICD due to inhibition of the CCL2-CCR2 pathway was accompanied by attenuated accumulation of innate immune cells. However, the contribution of innate immune cell infiltration to the development of SDS-induced ICD is unclear, as cutaneous CCL2-CCR2 signaling might induce ICD by the activation of skin-resident cells, such as keratinocytes, independently of innate immune cell accumulation. In addition, monocytes were not required for the development of SDS-induced ICD, despite marked accumulation in the lesional skin. We therefore examined whether the *in vivo* depletion of neutrophils affects the development of SDS-induced ICD. The specific and efficient depletion of neutrophils in the peripheral blood was achieved by the administration of rat anti-Ly6G Ab in combination with mouse anti-rat IgG Ab every other day, as described previously, with some modifications (Figure 5a and Supplementary Figure S6a) (Boivin et al. 2020). SDS-induced ear swelling, epidermal thickening, and increased TEWL were significantly milder in anti-Ly6G Ab-treated mice than in isotype control Ab-treated mice (Figure 5b-d), suggesting an important role of neutrophils in this model. Flow cytometric analysis revealed that the SDS-induced accumulation of neutrophils, monocytes, and eosinophils was significantly reduced by anti-Ly6G-mediated

neutrophil depletion (Figure 5e and Supplementary Figure S6b), suggesting that neutrophil infiltration in SDS-treated skin promoted the recruitment of monocytes and eosinophils. Thus, it is likely that CCL2-CCR2 signaling in the SDS-treated skin promoted the development of ICD, at least in part by inducing neutrophil accumulation in the lesional skin.

Impaired IL-1β production was responsible for the attenuation of neutrophil accumulation and SDS-induced ICD in *Ccr2*$^{-/-}$ mice

Lastly, we investigated how neutrophil infiltration in SDS-treated skin was controlled by cutaneous CCL2-CCR2 signaling by RNA-seq analysis of SDS-treated skin in WT and *Ccr2*$^{-/-}$ mice. Based on a gene set enrichment analysis, we identified differentially expressed pathways, including a neutrophil migration-associated gene set (GO:1990266), which was downregulated in *Ccr2*$^{-/-}$ mice (Figure 6a, Supplementary Table S1 and S2). The downregulated genes included *Il1b* as well as genes encoding neutrophil chemo-attractants, such as *Cxcl1, Cxcl2,* and *Cxcl5* (Figure 6b). The *Il1b* gene was strongly downregulated in *Ccr2*$^{-/-}$ mice (Figure 6c and Supplementary Table S3). Similar results were obtained by a comparative RNA-seq analysis of WT mice reconstituted with WT BM cells and *Ccr2*$^{-/-}$ mice reconstituted with WT BM cells (Supplementary Figure S7a-c and Supplementary Table S4-6).

It has been suggested that IL-1β can potently recruit neutrophils by inducing the production of various neutrophil chemoattractants (Biondo et al. 2014; Oliveira et al. 2008). We thus hypothesized that low IL-1β expression in the SDS-treated skin of

Ccr2$^{-/-}$ mice might result in impaired neutrophil accumulation, leading to the amelioration of ICD. To evaluate this hypothesis, we first examined the consequences of IL-1β neutralization on SDS-treated skin. SDS-induced ear swelling and neutrophil accumulation were significantly attenuated by the intradermal injection of an anti-IL-1β neutralizing Ab (Figure 6d and e). Next, we examined whether the amelioration of SDS-induced ICD in *Ccr2*$^{-/-}$ mice could be reversed by supplementation with exogenous IL-1β. Either PBS or recombinant murine IL-1β was intradermally injected into the ears of WT and *Ccr2*$^{-/-}$ mice on day 2 of the 6-day SDS application period. We observed that the attenuation of SDS-induced ear swelling in *Ccr2*$^{-/-}$ mice was reversed by the local injection of IL-1β (Figure 6f). The impaired accumulation of neutrophils in the SDS-treated skin of *Ccr2*$^{-/-}$ mice was also reversed by IL-1β injection (Figure 6g). These results suggest that CCR2-dependent IL-1β expression in the SDS-treated skin was critical for lesional neutrophil accumulation and the development of ICD.

Finally, to identify the cell sources of IL-1β, we examined whether IL-1β-expressing cells were co-stained with vimentin or CD45 by immunohistochemistry. More IL-1β-expressing cells were detected in SDS-treated skin on day 4 than on day 0 (Figure 6h). The majority of IL-1β-expressing cells were positive for vimentin while few IL-1β-expressing cells were CD45-positive (Figure 6h and Supplementary Figure S8). Moreover, IL-1β/vimentin double-positive cells were also detected in lesional skin of human cumulative ICD (Supplementary Figure S9).

These results suggest that IL-1β is produced in the lesional skin of cumulative ICD, preferentially by mesenchymal cells.

Discussion

In the present study, we identified a critical cytokine/chemokine signaling pathway in the skin for the control of innate skin responses to cumulative irritation by a surfactant, SDS. We found that CCL2-CCR2 signaling in the skin is essential for the development of SDS-induced ICD. Our results further suggest that CCR2-dependent IL-1β production in SDS-treated skin induces the development of ICD, at least in part by promoting neutrophil accumulation (see Graphical Abstract).

CCL2-CCR2 signaling is essential for the recruitment of circulating $CCR2^+$ cells, in particular monocytes, to peripheral tissues, including the skin (Kurihara et al. 1997; Talbot et al. 2015; Terwey et al. 2005; Tsou et al. 2007; Vanbervliet et al. 2002). However, our data suggest that the development of SDS-induced ICD depends on CCR2 signaling in the radioresistant compartment of the skin and not in radiosensitive circulating hematopoietic cells, including monocytes. Several previous studies have suggested that CCL2 has non-chemoattractant functions on radioresistant cells, such as mast cell degranulation (Campbell et al. 1999), cell adhesion molecule upregulation in fibroblasts (Lin et al. 2012), the modulation of endothelial cell function associated with cell extravasation and vascular permeability (Stamatovic et al. 2003), and the activation of a subset of dorsal root ganglion neurons associated with itch- and pain-related behaviors (Jiang et al. 2019). Thus, although we failed to detect

CCR2-expressing radioresistant cells in SDS-treated skin by either immunohistochemistry or RNA *in situ* hybridization in this study (data not shown), it is possible that the effects of CCL2 on one or more of these cell types lead to neutrophil accumulation and the development of SDS-induced ICD.

We showed that the development of SDS-induced ICD depends on the lesional accumulation of neutrophils but not monocytes, although both cell types were abundant in lesions. Our results further suggest that neutrophil accumulation in SDS-treated skin is mediated by CCR2-dependent IL-1β production. Accumulating evidence suggests that local IL-1β production can promote neutrophil recruitment in both humans and mice (Faccioli et al. 1990; Lappalainen et al. 2005; Miller et al. 2007; Nakamura et al. 2009). In addition, it has been demonstrated that IL-1β promotes neutrophil migration by priming neutrophils and inducing the production of neutrophil chemoattractants (Biondo et al. 2014; Oliveira et al. 2008). These mechanisms may contribute to IL-1β-mediated neutrophil accumulation in SDS-treated skin.

We revealed that SDS-induced IL-1β production in the skin depends on CCR2 in radioresistant cells, but the underlying mechanism remains to be elucidated. Immunohistochemical analyses suggested that IL-1β in SDS-treated skin is produced preferentially by mesenchymal cells. Given that mesenchymal cells are radioresistant, their IL-1β expression may be upregulated directly via CCR2 on their surface or induced by signals emanated from radioresistant cells activated via CCR2.

Our results also suggest that the development of SDS-induced ICD is independent of either basophils or $CD4^+$ T cells, different from previous results showing that these

cells contribute to the development of croton oil-induced acute ICD in mice (Kondo et al. 1996; Nakashima et al. 2014). This difference among studies can potentially be explained by multiple factors, such as the causal irritants and exposure duration (Patrick et al. 1987; Watkins and Maibach 2009). Thus, future studies are required to reveal whether the findings of this study are generalizable to ICD induced by different mechanisms.

In conclusion, we revealed that CCL2 and IL-1β are the key mediators in the skin critical for the development of SDS-induced ICD. Our results suggest that CCL2-CCR2 signaling in the skin drives SDS-induced ICD via IL-1β-mediated neutrophil accumulation in mice. This study may contribute to the development of improved management strategies for ICD and provide insights into the fundamental immune responses of the skin to external insults.

MATERIALS AND METHODS

Detailed experimental procedures are described in Supplementary Materials and Methods.

Mice

C57BL/6J mice were purchased from Charles River Laboratories Japan (Kanagawa, Japan). *E2a*^{Cre}, *Ccl2*$^{fl/fl}$, and *Ccr2*$^{-/-}$ mice were from Jackson Laboratory (Bar Harbor, ME, USA). 7- to 10-week-old male mice were used for all the experiments under specific pathogen-free conditions.

Induction of ICD

Anesthetized mice were treated topically with 20 μL of PBS and 2% (vol/vol) SDS (Sigma-Aldrich, St. Louis, MO, USA) on the right and left ear skin, respectively, for 6 consecutive days, unless otherwise stated.

Human skin samples

A healthy skin sample was obtained from a non-involved part of the triangular end of the surgically removed benign tumor on the forearm. A lesional skin specimen was obtained from a skin biopsy sample in the forearm of a patient with cumulative ICD caused by the intensive use of an ethanol-based sanitizer. This study was approved by the ethics committee of the Kyoto University Graduate School of Medicine (R0743) and written informed consent was obtained from individuals.

Generation of BM chimeric mice

BM chimeric mice were generated as previously described (Otsuka et al. 2010). Briefly, recipient mice were lethally X-irradiated (9.5 Gy) and were received BM cells (3 x 10^6 cells) intravenously 3 h after irradiation. The chimeric mice were used for the indicated experiment 12 weeks after transplantation.

Parabiosis

Pairs of parabiotic mice were generated, as described previously (Conboy et al. 2013; Duyverman et al. 2012). Topical application of SDS or PBS on the ears of parabionts was commenced 2 weeks after the surgical joining.

DATA AVAILABILITY STATEMENT

Raw sequence reads are deposited in the Sequence Read Archive (https://www.ncbi.nlm.nih.gov/sra) under accession numbers PRJNA722315 and PRJNA722317.

ORCIDs:

Rintaro Shibuya: https://orcid.org/0000-0003-3805-2562

Yoshihiro Ishida: https://orcid.org/0000-0002-6210-5903

Sho Hanakawa: https://orcid.org/0000-0002-0665-9602

Tatsuki R Kataoka: https://orcid.org/0000-0003-3095-8976

Yasuhide Takeuchi: https://orcid.org/0000-0002-1262-2355

Teruasa Murata: https://orcid.org/0000-0001-8350-1289

Arisa Akagi: https://orcid.org/0000-0003-3285-8995

Zachary Chow: https://orcid.org/0000-0003-4493-8730

Toshiaki Kogame: https://orcid.org/0000-0002-0683-719X

Satoshi Nakamizo: https://orcid.org/0000-0001-9332-0369

Saeko Nakajima: https://orcid.org/0000-0003-0831-1447

Gyohei Egawa: https://orcid.org/0000-0002-6101-4719

Takashi Nomura: https://orcid.org/0000-0002-4004-1339

Naotomo Kambe: https://orcid.org/0000-0001-9610-4952

Akihiko Kitoh: https://orcid.org/0000-0003-4724-8807

Kenji Kabashima: https://orcid.org/0000-0002-0773-0554

CONFLICT OF INTEREST

We state no conflict of interest.

AUTHOR CONTRIBUTIONS

Conceptualization: RS, AK; Formal Analysis: RS, AK, YI; Funding Acquisition: RS, KK; Investigation: RS, YI, TK, YT; Project Administration: RS, AK, KK; Methodology: RS, AK, YI; Supervision: KK; Validation: RS, SH, YI; Visualization: RS, YI; Writing-Original Draft Preparation: RS, AK; Writing-Review and Editing: RS, AK, YI, SH, TM, AA, ZC, TK, YT, SN, SN, GE, TN, NK, KK.

ACKNOWLEDGEMENTS

We thank Dr. Tomoyuki Furuyashiki (Kobe University) for providing *E2a*^{Cre} mice and Dr. Hanako Ikeda (Kyoto University) for *Ccr2*$^{-/-}$ mice, and members of Kabashima laboratory for their helpful discussion and support. This work was supported by JSPS KAKENHI [grant numbers 20K17317 (R.S.), 15H05790, 15H1155, 15K15417, and 20H05697 (K.K.)], and AMED [grant numbers JP17ek0410040 (S.N.) and JP20gm1210006 (K.K.)].

References

Akdis CA, Akdis M, Bieber T, Bindslev-Jensen C, Boguniewicz M, Eigenmann P, et al. Diagnosis and treatment of atopic dermatitis in children and adults: European Academy of Allergology and Clinical Immunology/American Academy of Allergy, Asthma and Immunology/PRACTALL Consensus Report. J. Allergy Clin. Immunol. 2006;118(1):152–69

Anderson C, Sundberg K, Groth O. Animal model for assessment of skin irritancy. Contact Dermatitis. 1986;15(3):143–51

Andres RH, Choi R, Pendharkar A V., Gaeta X, Wang N, Nathan JK, et al. The CCR2/CCL2 interaction mediates the transendothelial recruitment of intravascularly delivered neural stem cells to the ischemic brain. Stroke. 2011;42(10):2923–31

Arai M, Ikawa Y, Chujo S, Hamaguchi Y, Ishida W, Shirasaki F, et al. Chemokine receptors CCR2 and CX3CR1 regulate skin fibrosis in the mouse model of cytokine-induced systemic sclerosis. J. Dermatol. Sci. Japanese Society for Investigative Dermatology; 2013;69(3):250–8

Berg DJ, Leach MW, Kühn R, Rajewsky K, Müller W, Davidson NJ, et al. Interleukin 10 but not interleukin 4 is a natural suppressant of cutaneous inflammatory responses. J. Exp. Med. 1995;182(1):99–108

Biondo C, Mancuso G, Midiri A, Signorino G, Domina M, Lanza Cariccio V, et al. The interleukin-1β/CXCL1/2/neutrophil axis mediates host protection against group B streptococcal infection. Infect. Immun. 2014;82(11):4508–17

Boivin G, Faget J, Ancey PB, Gkasti A, Mussard J, Engblom C, et al. Durable and controlled depletion of neutrophils in mice. Nat. Commun. 2020;11(1):1–9

Calhoun KN, Luckett-Chastain LR, Frempah B, Gallucci RM. Associations Between Immune Phenotype and Inflammation in Murine Models of Irritant Contact Dermatitis. Toxicol. Sci. 2019;168(1):179–89

Campbell EM, Charo IF, Kunkel SL, Strieter RM, Boring L, Gosling J, et al. Monocyte chemoattractant protein-1 mediates cockroach allergen-induced bronchial hyperreactivity in normal but not CCR2-/- mice: the role of mast cells. J. Immunol. 1999;163(4):2160–7

Cohen, E. D. Irritant contact dermatitis. In: Bolognia J, Schaffer J, Cerroni L, editors. Dermatology. 4th ed. Edinburgh: Elsevier Ltd; 2018. p. 262–73

Conboy MJ, Conboy IM, Rando TA. Heterochronic parabiosis: Historical perspective and methodological considerations for studies of aging and longevity. Aging Cell. 2013;12(3):525–30

Dickel H, Bruckner T, Bernhard-Klimt C, Koch T, Scheidt R, Diepgen TL. Surveillance scheme for occupational skin disease in the Saarland, FRG: First report from BKH-S. Contact Dermatitis. 2002;46(4):197–206

Dietz JB, Menné T, Meyer HW, Viskum S, Flyvholm MA, Ahrensbøll-Friis U, et al. Degree of employment, sick leave, and costs following notification of occupational contact dermatitis—A register-based study. Contact Dermatitis. 2020;(July):1–12

Dimitrijevic OB, Stamatovic SM, Keep RF, Andjelkovic A V. Absence of the chemokine receptor CCR2 protects against cerebral ischemia/reperfusion injury in mice. Stroke. 2007;38(4):1345–53

Duyverman AMMJ, Kohno M, Duda DG, Jain RK, Fukumura D. A transient parabiosis skin transplantation model in mice. Nat. Protoc. Nature Publishing Group; 2012;7(4):763–70

Faccioli LH, Souza GEP, Cunha FQ, Poole S, Ferreira SH. Recombinant interleukin-1 and tumor necrosis factor induce neutrophil migration “in vivo” by indirect mechanisms. Agents Actions. 1990;30(3–4):344–9

Gittler JK, Krueger JG, Guttman-Yassky E. Atopic dermatitis results in intrinsic barrier and immune abnormalities: Implications for contact dermatitis. J. Allergy Clin. Immunol. Elsevier Ltd; 2013;131(2):300–13

Ishida Y, Kuninaka Y, Nosaka M, Furuta M, Kimura A, Taruya A, et al. CCL2-Mediated Reversal of Impaired Skin Wound Healing in Diabetic Mice by Normalization of Neovascularization and Collagen Accumulation. J. Invest. Dermatol. Society for Investigative Dermatology; 2019;139(12):2517-2527.e5

Jiang H, Cui H, Wang T, Shimada SG, Sun R, Tan Z, et al. CCL2/CCR2 signaling elicits itch- and pain-like behavior in a murine model of allergic contact dermatitis. Brain. Behav. Immun. Elsevier; 2019;80(April):464–73

Kashyap S, Osman M, Ferguson CM, Nath MC, Roy B, Lien KR, et al. Ccl2 deficiency protects against chronic renal injury in murine renovascular hypertension. Sci. Rep. 2018;8(1):1–12

Kondo S, Beissert S, Wang B, Fujisawa H, Kooshesh F, Stratigos A, et al. Hyporesponsiveness in contact hypersensitivity and irritant contact dermatitis in CD4 gene targeted mouse. J. Invest. Dermatol. Elsevier Masson SAS; 1996;106(5):993–1000

Kurihara T, Warr G, Loy J, Bravo R. Defects in Macrophage Recruitment and Host Defense in Mice Lacking the CCR2 Chemokine Receptor. J. Exp. Med. 1997;186(10):1757–62

Lappalainen U, Whitsett JA, Wert SE, Tichelaar JW, Bry K. Interleukin-1β causes pulmonary inflammation, emphysema, and airway remodeling in the adult murine lung. Am. J. Respir. Cell Mol. Biol. 2005;32(4):311–8

Lee EG, Mickle-Kawar BM, Gallucci RM. IL-6 deficiency exacerbates skin inflammation in a murine model of irritant dermatitis. J. Immunotoxicol. 2013;10(2):192–200

Lin YM, Hsu CJ, Liao YY, Chou MC, Tang CH. The CCL2/CCR2 Axis Enhances Vascular Cell Adhesion Molecule-1 Expression in Human Synovial Fibroblasts. PLoS One. 2012;7(11):1–10

Meller S, Lauerma AI, Kopp FM, Winterberg F, Anthoni M, Müller A, et al. Chemokine responses distinguish chemical-induced allergic from irritant skin inflammation: Memory T cells make the difference. J. Allergy Clin. Immunol. 2007;119(6):1470–80

Miller LS, Pietras EM, Uricchio LH, Hirano K, Rao S, Lin H, et al. Inflammasome-Mediated Production of IL-1β Is Required for Neutrophil Recruitment against Staphylococcus aureus In Vivo . J. Immunol. 2007;179(10):6933–42

Nakamura Y, Kambe N, Saito M, Nishikomori R, Kim YG, Murakami M, et al. Mast cells mediate neutrophil recruitment and vascular leakage through the NLRP3 inflammasome in histamine-independent urticaria. J. Exp. Med. 2009;206(5):1037–46

Nakashima C, Otsuka A, Kitoh A, Honda T, Egawa G, Nakajima S, et al. Basophils regulate the recruitment of eosinophils in a murine model of irritant contact dermatitis. J. Allergy Clin. Immunol. Elsevier Ltd; 2014;134(1):100-107.e12

Oliveira SHP, Canetti C, Ribeiro RA, Cunha FQ. Neutrophil migration induced by IL-1β depends upon LTB4 released by macrophages and upon TNF-α and IL-1β released by mast cells. Inflammation. 2008;31(1):36–46

Otsuka K, Hirabayashi Y, Tsuboi I, Inoue T. Regeneration capability of Lin-/c-Kit+/Sca-1+ cells with or without radiation exposure for repopulation of peripheral blood in lethally irradiated mice monitored using Ly5.1 isotype on days 35, 90, and 270 after transplantation. Exp. Hematol. ISEH - Society for Hematology and Stem Cells; 2010;38(5):417–25

Patrick E, Burkhalter A, Maibach HI. Recent investigations of mechanisms of chemically induced skin irritation in laboratory mice. J. Invest. Dermatol. 1987;88(3 SUPPL.):24–31

Piguet PF. Tumor necrosis factor is a critical mediator in hapten induced irritant and contact hypersensitivity reactions. J. Exp. Med. 1991;173(3):673–9

Slodownik D, Lee A, Nixon R. Irritant contact dermatitis: A review. Australas. J. Dermatol. 2008;49(1):1–11

Stamatovic SM, Keep RF, Kunkel SL, Andjelkovic A V. Potential role of MCP-1 in endothelial cell tight junction “opening”: Signaling via Rho and Rho kinase. J. Cell Sci. 2003;116(22):4615–28

Talbot J, Bianchini FJ, Nascimento DC, Oliveira RDR, Souto FO, Pinto LG, et al. CCR2 expression in neutrophils plays a critical role in their migration into the joints in rheumatoid arthritis. Arthritis Rheumatol. 2015;67(7):1751–9

Terwey TH, Kim TD, Kochman AA, Hubbard VM, Lu S, Zakrzewski JL, et al. CCR2 is required for CD8-induced graft-versus-host disease. Blood. 2005;106(9):3322–30

Tsou CL, Peters W, Si Y, Slaymaker S, Aslanian AM, Weisberg SP, et al. Critical roles for CCR2 and MCP-3 in monocyte mobilization from bone marrow and recruitment to inflammatory sites. J. Clin. Invest. 2007;117(4):902–9

Vanbervliet B, Homey B, Durand I, Massacrier C, Aït-Yahia S, De Bouteiller O, et al. Sequential involvement of CCR2 and CCR6 ligands for immature dendritic cell recruitment: Possible role at inflamed epithelial surfaces. Eur. J. Immunol. 2002;32(1):231–42

Watkins SA, Maibach HI. The hardening phenomenon in irritant contact dermatitis: An interpretative update. Contact Dermatitis. 2009;60(3):123–30

Weedon D. The spongiotic reaction pattern. Weedon's Ski. Pathol. 3rd ed. Edinburgh: Elsevier Ltd; 2010. p. 102–4

Willenborg S, Lucas T, Van Loo G, Knipper JA, Krieg T, Haase I, et al. CCR2 recruits an inflammatory macrophage subpopulation critical for angiogenesis in tissue repair. Blood. 2012;120(3):613–25

Williams J, Cahill J, Nixon R. Occupational autoeczematization or atopic eczema precipitated by occupational contact dermatitis? Contact Dermatitis. 2007;56(1):21–6

Zhang J, Xu P, Song P, Wang H, Zhang Y, Hu Q, et al. CCL2-CCR2 signaling promotes hepatic ischemia/reperfusion injury. J. Surg. Res. United States; 2016;202(2):352–62

Figure legends

Figure 1. Repeated topical application of SDS induced cumulative ICD in mice.

(**a–e, g**) PBS or SDS was topically applied to the ears of WT mice for 6 consecutive days (n = 5). (**a**) Phenotypical appearance. Representative photographs are shown. (**b**) Kinetics of ear swelling. Days on x-axis refer to days after start of the treatment. (**c**) TEWL. (**d**) Hematoxylin and eosin staining of sections from PBS- and SDS-treated skin. Representative photomicrographs are shown. Scale bars = 50 μm. (**e**) Epidermal thickness. (**f**) Hematoxylin and eosin staining of sections of lesional skin from a patient with cumulative ICD and site-matched skin from a healthy subject. Representative photomicrographs are shown. Scale bars = 200 μm. (**g**) Total cell numbers for the indicated subsets in PBS- and SDS-treated ear skin were determined by flow cytometry. *P < 0.05, **P < 0.01, ****P < 0.0001. Data are shown as values (*symbols*) and means ± SDs (*bars*). ns, Not significant. d, day.

Figure 2. Locally produced CCL2 was required for the development of SDS-induced ICD.

(a) SDS was topically applied to the ears of WT mice for 2 to 6 consecutive days (n = 5 per group). *Ccl2* mRNA expression levels in non-treated (d0) and SDS-treated (d2, d4, and d6) ear skin were evaluated by quantitative reverse transcription polymerase chain reaction. Data are representative of 2 experiments. A.U., arbitrary unit. **(b)** PBS or SDS was topically applied to the ears of WT mice (n = 5) for 6 consecutive days.

Protein levels of CCL2 in PBS- or SDS-treated ear skin were assessed by ELISA. **(c)** SDS was topically applied to the ears of WT mice for 4 consecutive days (n = 5). Non-treated (d0) and SDS-treated (d4) ear skin samples were subjected to RNA *in situ* hybridization (RNAscope) of *Ccl2* in combination with immunofluorescence staining for vimentin. Representative images are shown. Scale bars = 20 μm. DAPI, 4',6-diamidino-2-phenylindole. White circles indicate *Ccl2*/vimentin-double positive cells. **(d)** Samples from lesional skin of a patient with cumulative ICD and site-matched skin of a healthy subject were subjected to RNA *in situ* hybridization (RNAscope) of *CCL2* in combination with immunofluorescence staining for vimentin. Representative images are shown. Scale bars = 50 μm. White circles indicate *CCL2*/vimentin-double positive cells. (**e–h**) PBS or SDS was topically applied to the ears of $Ccl2^{fl/fl}$ (n = 6) and $Ccl2^{fl/fl}E2a^{Cre}$ (n = 4) mice for 6 consecutive days. Kinetics of ear swelling (**e**), epidermal thickness (**f**), TEWL (**g**), and total cell numbers of the indicated subsets in the ear skin (**h**) are shown. Data are representative of two experiments. (**i, j**) WT mice (n = 4) were treated topically with SDS on both ears for 6 consecutive days, with the intradermal administration of 20 μg of isotype IgG (left ears) and anti-CCL2 Ab (right ears) on d0, d2, and d4. Kinetics of ear swelling (**h**) and total cell numbers of the indicated subsets in the ear skin (**i**) are shown. Data are representative of two experiments and shown as values (*symbols*) and means ± SDs (*bars*). *P < 0.05, **P < 0.01, ***P < 0.001. ns, Not significant. d, day.

Figure 3. CCR2 deficiency in radiosensitive hematopoietic cells did not affect the development of SDS-induced ICD.

(**a–d**) PBS or SDS was topically applied to the ears of WT (n = 5) and *Ccr2*$^{-/-}$ (n = 5) mice for 6 consecutive days. Kinetics of ear swelling (**a**), epidermal thickness (**b**), TEWL (**c**), and total cell numbers of the indicated subsets in the ear skin (**d**) are shown. (**e**) Schematic representation of BM chimera generation and ICD induction. Lethally irradiated WT mice were transplanted with WT or *Ccr2*$^{-/-}$ BM cells. Twelve weeks later, PBS or SDS was topically applied to the ears of WT BM-transplanted (n = 6) and *Ccr2*$^{-/-}$ BM-transplanted (n = 4) mice for 6 consecutive days. (**f**) Total cell numbers of the indicated subsets in the ear skin. (**g**) Kinetics of ear swelling. Days on x-axis refer to days after start of the treatment. (**h**) Epidermal thickness. (**i**) TEWL. Data are shown as values (*symbols*) and means ± SDs (*bars*). **P < 0.01, ****P < 0.0001. ns, Not significant. d, day.

Figure 4. CCR2 signaling in the radioresistant compartment of the skin was required for the development of SDS-induced ICD.

(**a**) Schematic representation of BM chimera generation and ICD induction. Lethally irradiated WT (n = 6) or *Ccr2*$^{-/-}$ (n = 4) mice were transplanted with WT BM cells. Twelve weeks later, PBS or SDS was topically applied to the ears of BM-transplanted mice for 6 consecutive days. (**b**) Kinetics of ear swelling. Days on x-axis refer to days after start of the treatment. (**c**) Epidermal thickness. (**d**) TEWL. (**e**) Total cell numbers of the indicated subsets in the skin. (**f**) Schematic representation of parabiosis and ICD

induction. WT and *Ccr2*$^{-/-}$ mice were surgically joined to share blood circulation (parabiosis) (n = 9). Two weeks later, PBS or SDS was topically applied to the ears of both parabionts for 6 consecutive days. (**g**) Kinetics of ear swelling. Days on x-axis refer to days after start of the treatment. (**h**) Total cell numbers of the indicated subsets in the ear skin. Data are shown as values (*symbols*) and means ± SDs (*bars*). Results from a total of three independent experiments are shown. *P < 0.05, **P < 0.01, ***P < 0.001. ns, Not significant. d, day.

Figure 5. Neutrophil deficiency resulted in the amelioration of SDS-induced ICD.

WT mice were treated topically with PBS and SDS on the right and left ears, respectively, for 6 consecutive days, with the intraperitoneal injection of isotype rat IgG2a (n = 5) or rat anti-Ly6G Ab (IgG2a) (n = 5), followed by intraperitoneal injection of anti-rat IgG2a Ab on d-1, d1, d3, and d5. Cell numbers of the indicated subsets in the peripheral blood (**a**), kinetics of ear swelling (**b**), epidermal thickness (**c**), TEWL (**d**), and total cell numbers of the indicated subsets in the ear skin (**e**) are shown. Data are representative of two experiments and shown as values (*symbols*) and means ± SDs (*bars*). *P < 0.05, **P < 0.01, ***P < 0.001, ****P < 0.0001. ns, Not significant. d, day.

Figure 6. Impaired IL-1β production was responsible for the attenuation of neutrophil accumulation and SDS-induced ICD in *Ccr2*$^{-/-}$ mice.

(**a–c**) Analyses of RNA-seq data obtained from SDS-treated skin of WT (n = 3) and *Ccr2*$^{-/-}$ (n = 3) mice. Gene set enrichment analysis (**a**) and a heat map (**b**) of the GO_NEUTROPHIL_MIGRATION gene set (GO:1990266). Volcano plots comparing gene expression in WT and *Ccr2*$^{-/-}$ mice (**c**). (**d, e**) WT mice (n = 6) were treated topically with SDS on both ears for 6 consecutive days, with the intradermal administration of 20 μg of isotype IgG (left ears) and anti-IL-1β Ab (right ears) on d0, d2, and d4. Kinetics of ear swelling (**d**) and total numbers of neutrophils in the ear skin (**e**) are shown. Data are representative of two experiments. (**f, g)** PBS or SDS was topically applied to the ears of WT (n = 10) and *Ccr2*$^{-/-}$ mice (n = 9) for 6 consecutive days, with the intradermal (i.d.) injection of PBS or recombinant murine (rm) IL-1β (50 ng) on d2. Ear swelling (**f**) and total numbers of neutrophils in the ear skin (**g**) were analyzed on d6. Data are representative of two experiments and shown as values (*symbols*) and means ± SDs (*bars*). *P < 0.05, **P < 0.01, ***P < 0.001. ns, Not significant. d, day. **(h)** SDS was topically applied to the ears of WT mice for 4 consecutive days (n = 5). Expression of IL-1β and vimentin protein in non-treated (d0) and SDS-treated (d4) ear skin were examined by immunofluorescence. Representative images are shown. Scale bars = 20 μm. DAPI, 4’,6-diamidino-2-phenylindole. White circles indicate IL-1β/vimentin-double positive cells.

Figure 1.
Shibuya et al.

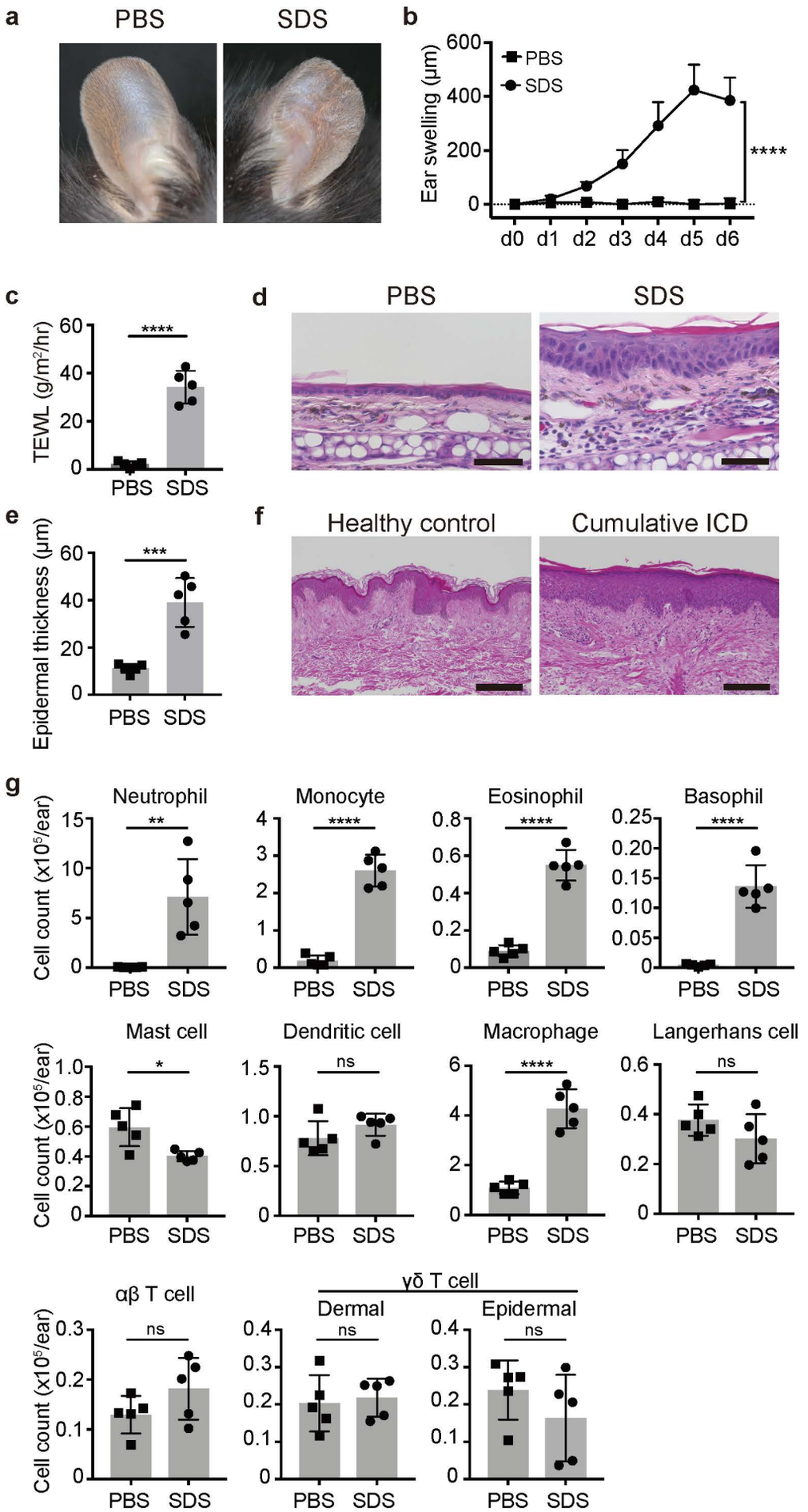

Figure 2.
Shibuya et al.

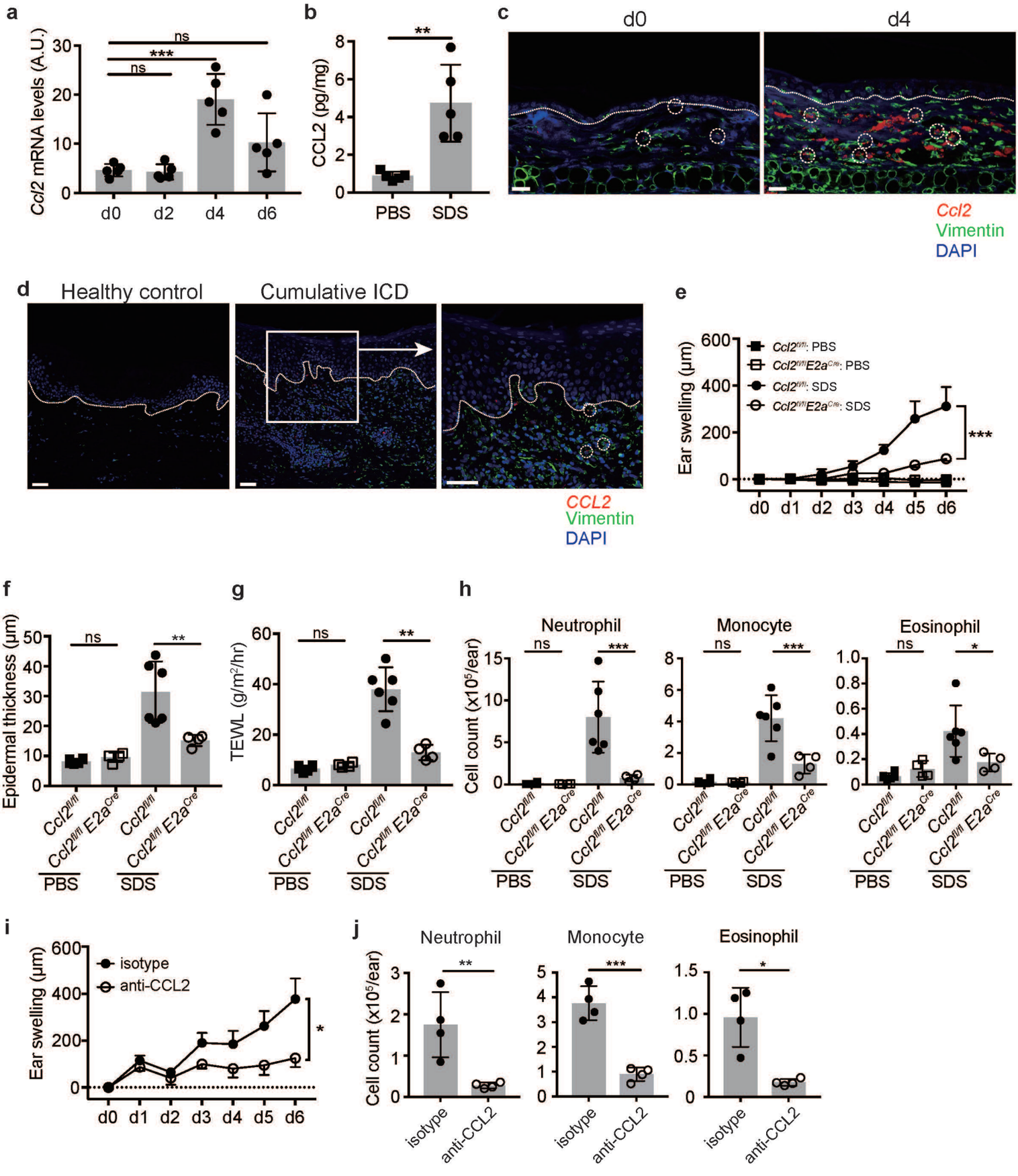

Figure 3.
Shibuya et al.

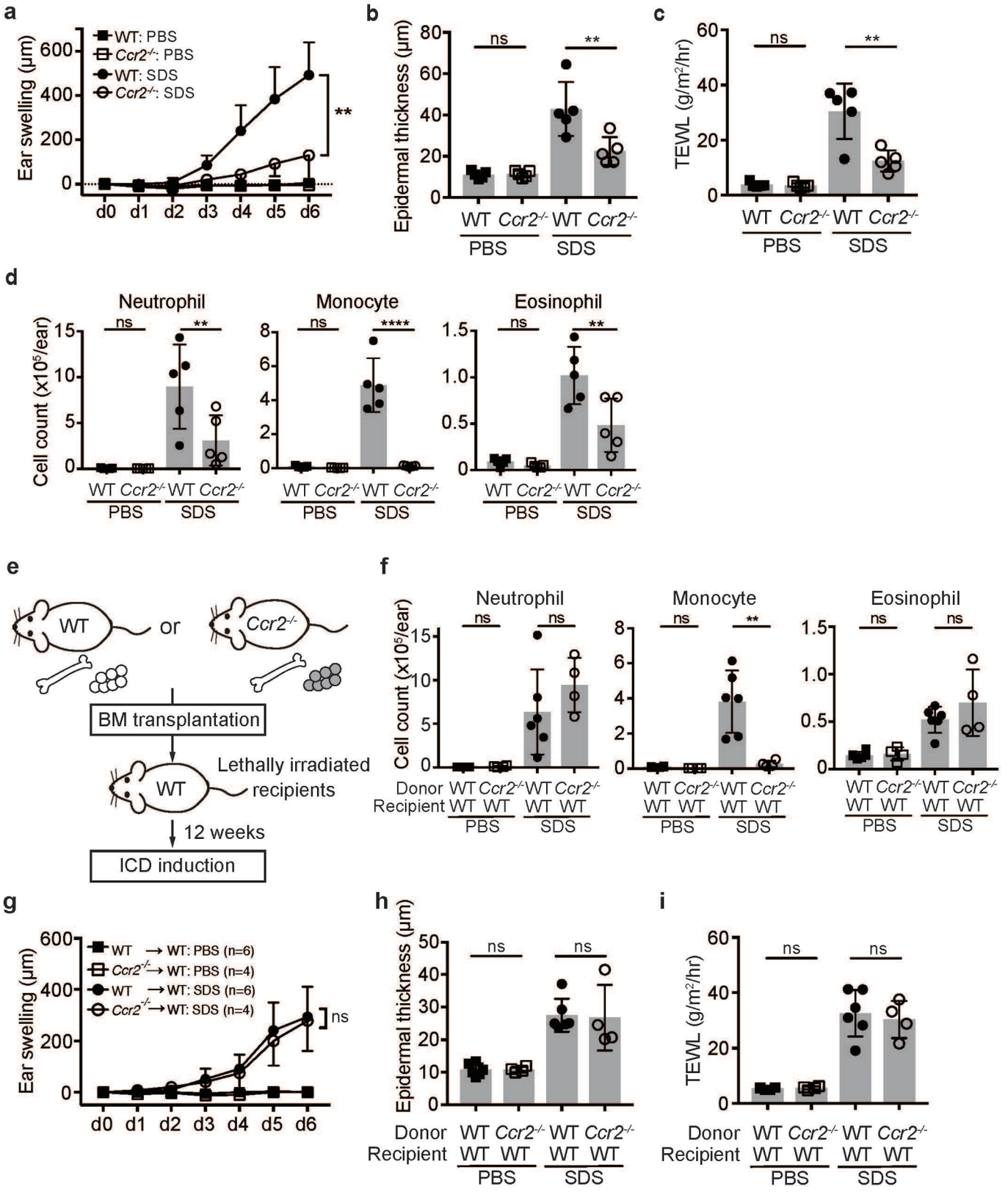

Figure 4.
Shibuya et al.

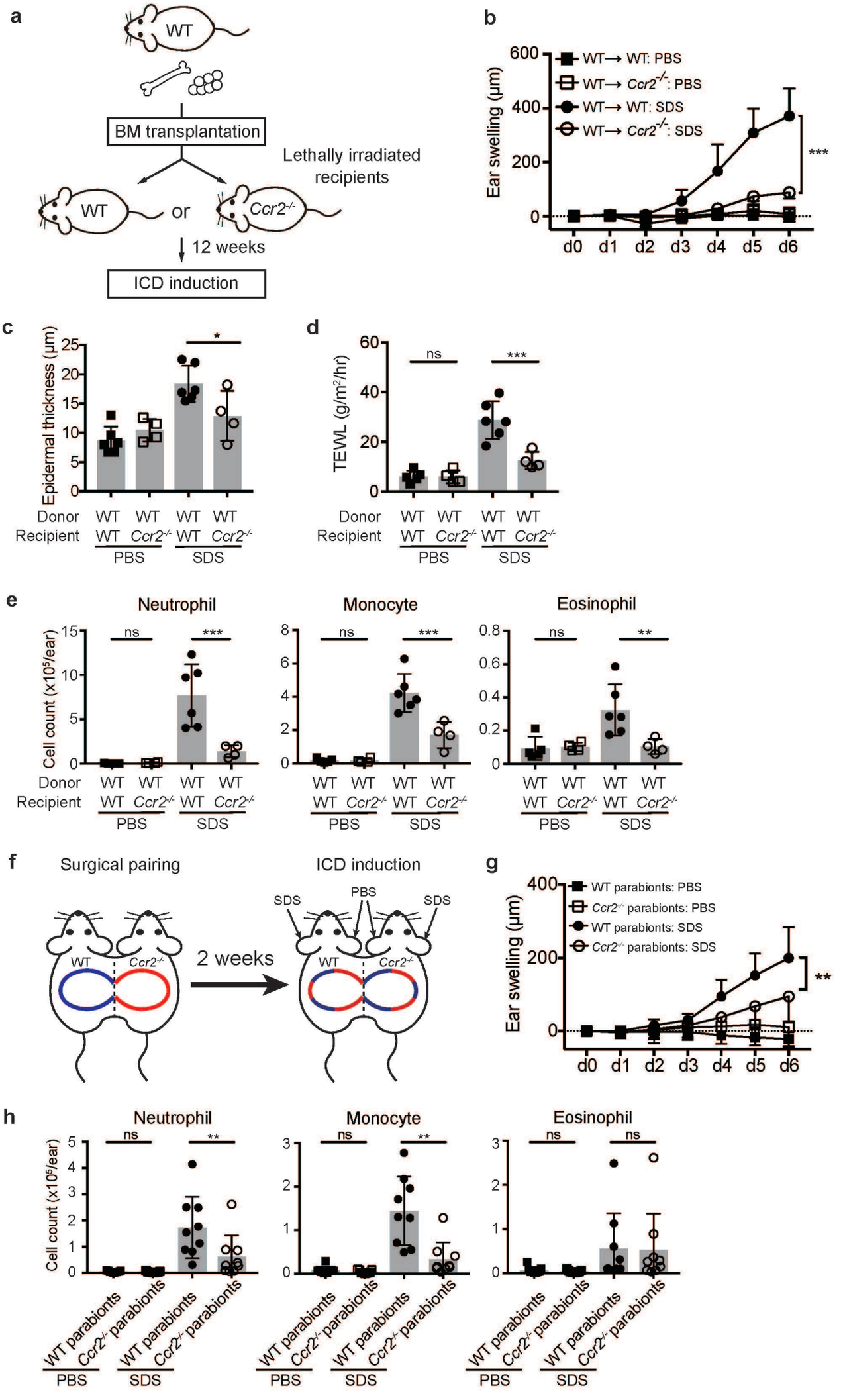

Figure 5.
Shibuya et al.

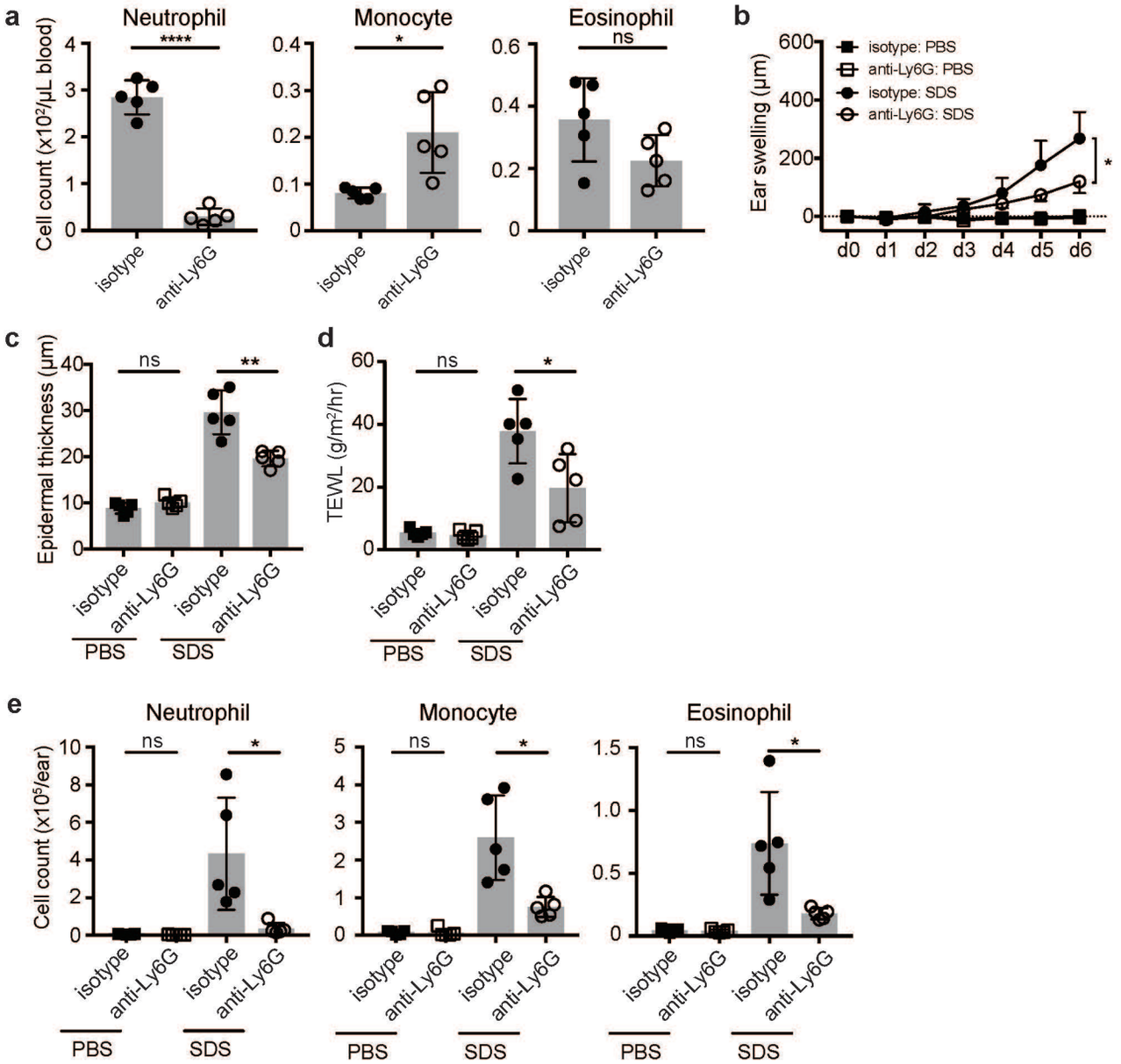

Figure 6.
Shibuya et al.

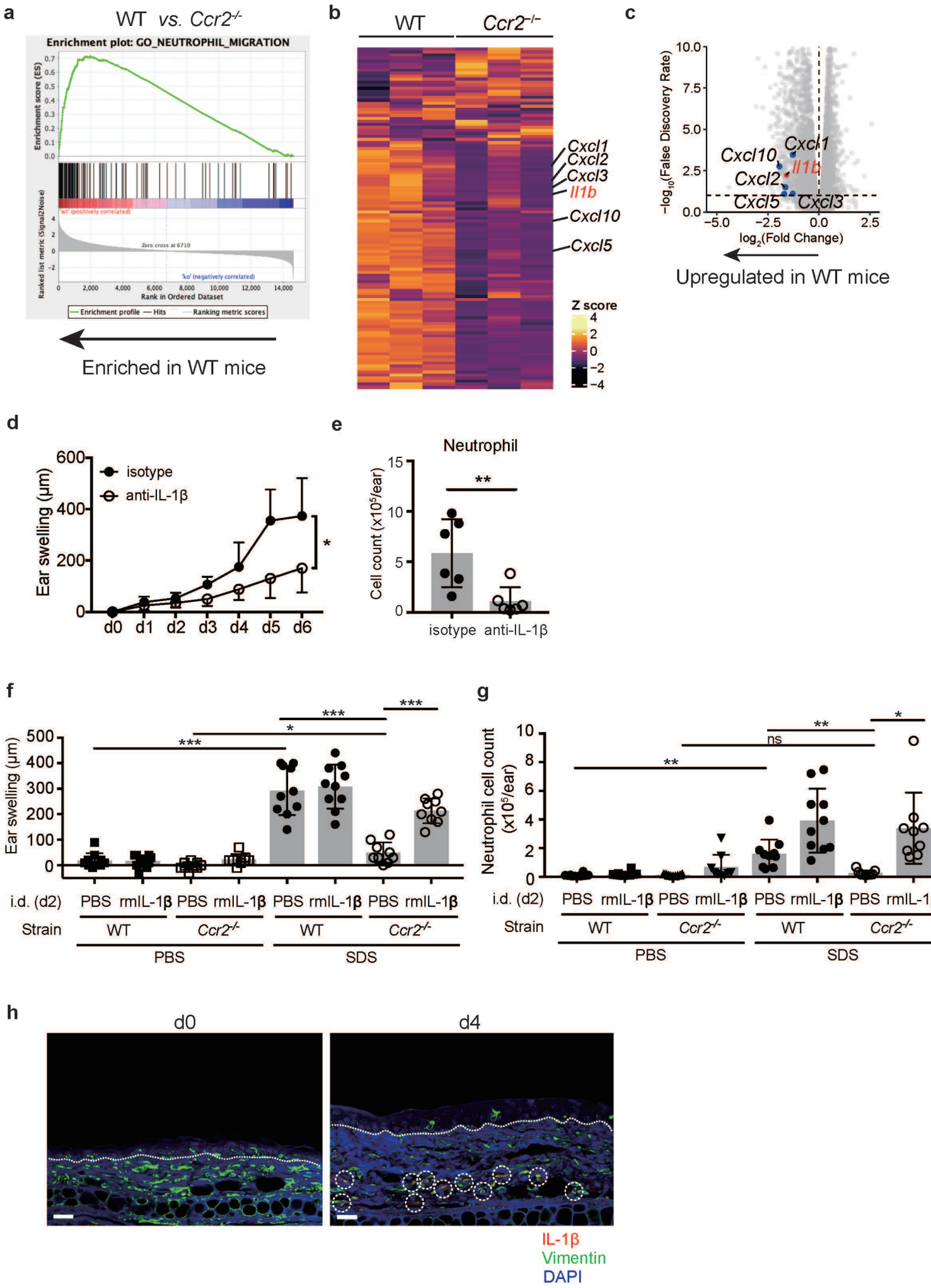

Graphic abstract

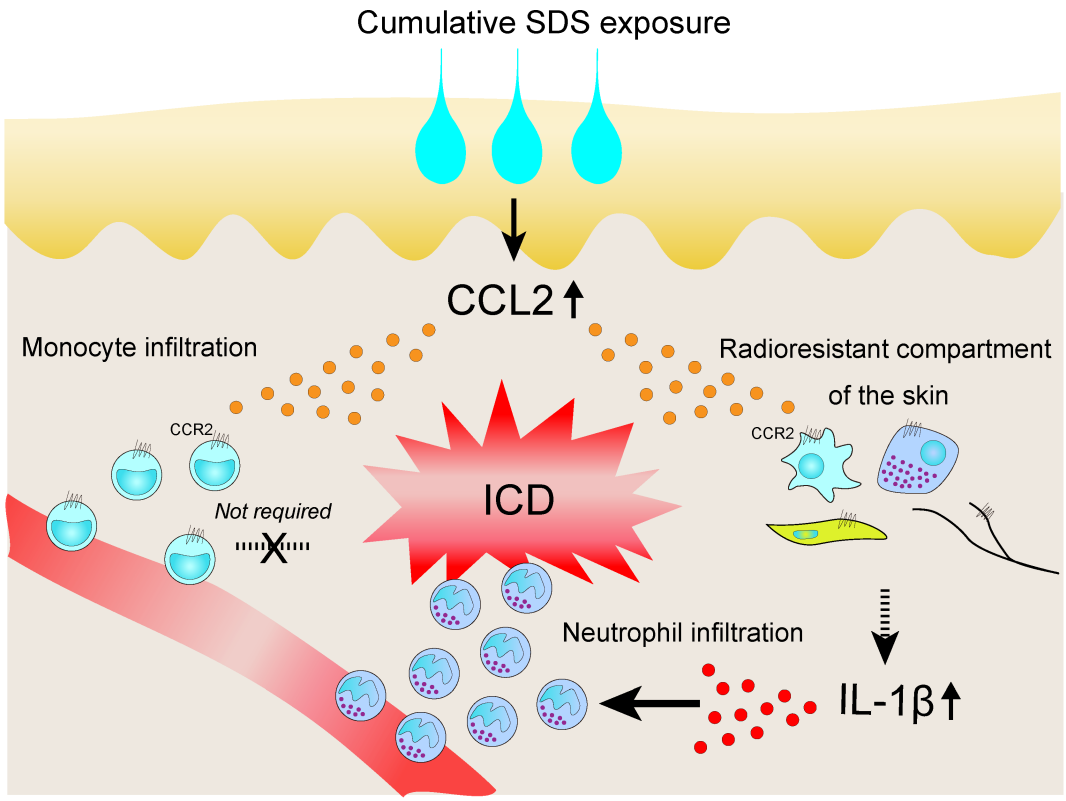

Supplementary Figures.

Supplementary Figure S1.
Shibuya et al.

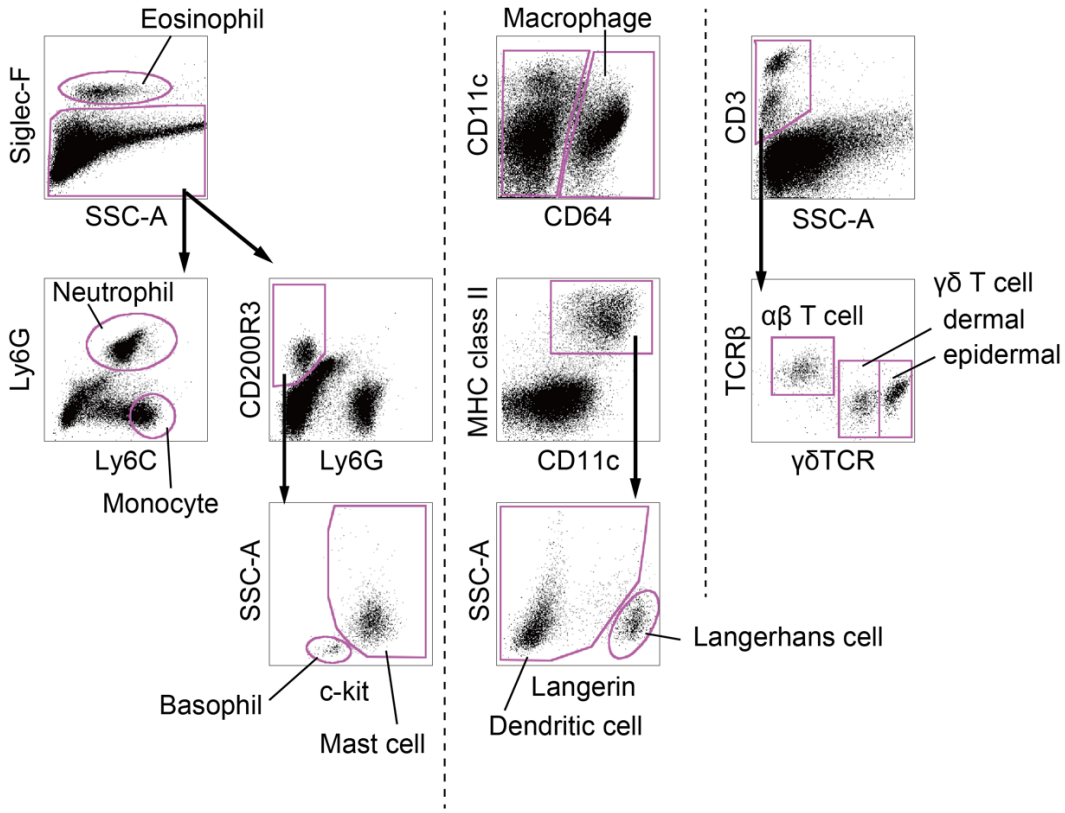

Supplementary Figure S1. Identification of cell infiltrates in SDS-treated skin.

SDS was topically applied to the ears of WT mice (n = 5) for 6 consecutive days. SDS-treated ear skin was analyzed by flow cytometry on day 6. Representative flow cytometry plots show the gating strategy for the following subsets from $CD45^+$ cells in SDS-treated skin: neutrophils (Siglec-F^-, $Ly6G^+$), monocytes (Siglec-F^-, $Ly6G^-$, $Ly6C^{high}$), eosinophils (Siglec-F^+), mast cells (Siglec-F^-, $CD200R3^+$, c-kit^+), basophils (Siglec-F^-, $CD200R3^+$, c-kit^-), macrophages ($CD64^+$), dendritic cells ($CD64^-$, $CD11c^+$, MHC class II^+, $Langerin^-$), Langerhans cells ($CD64^-$, $CD11c^+$, MHC class II^+, $Langerin^+$), αβ T cells ($CD3^+$, $TCR\beta^+$), dermal γδ T cells ($CD3^+$, $\gamma\delta TCR^{mid}$), and epidermal γδ T cells ($CD3^+$, $\gamma\delta TCR^{high}$).

Supplementary Figure S2.
Shibuya et al.

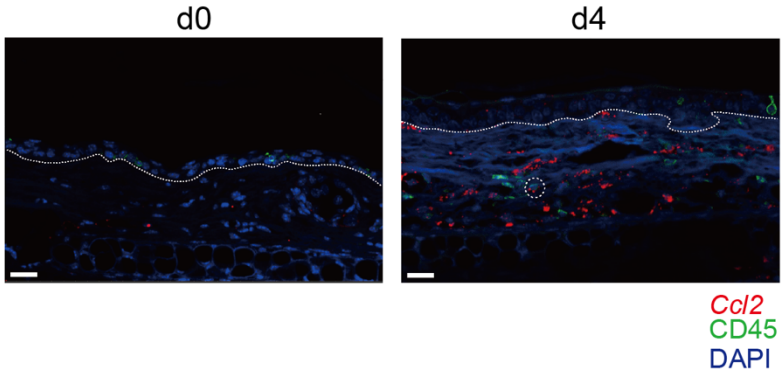

Supplementary Figure S2. Few *Ccl*2-positive cells expressed CD45 in SDS-treated ear skin.

SDS was topically applied to the ears of WT mice for 4 consecutive days (n = 5). Non-treated (d0) and SDS-treated (d4) ear skin samples were subjected to RNA *in situ* hybridization (RNAscope) of *Ccl2* in combination with immunofluorescence staining for CD45. Representative images are shown. Scale bars = 20 μm. DAPI, 4',6-diamidino-2-phenylindole. White circles indicate *Ccl2*/CD45-double positive cells.

Supplementary Figure S3.
Shibuya et al.

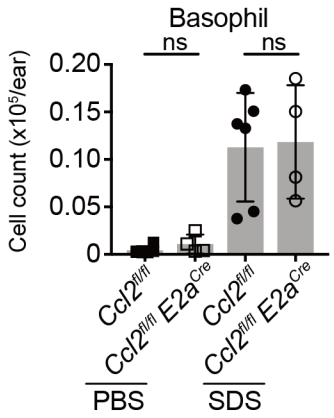

Supplementary Figure S3. Accumulation of basophils in SDS-treated skin was comparable between *Ccl2*$^{fl/fl}$ and *Ccl2*$^{fl/fl}$*E2a*^{Cre} mice.

PBS or SDS was topically applied to the ears of *Ccl2*$^{fl/fl}$ (n = 6) and *Ccl2*$^{fl/fl}$*E2a*^{Cre} (n = 4) mice for 6 consecutive days. Cell numbers of basophils in the skin were examined on day 6. Data are shown as values (*symbols*) and means ± SDs (*bars*). ns, Not significant.

Supplementary Figure S4.
Shibuya et al.

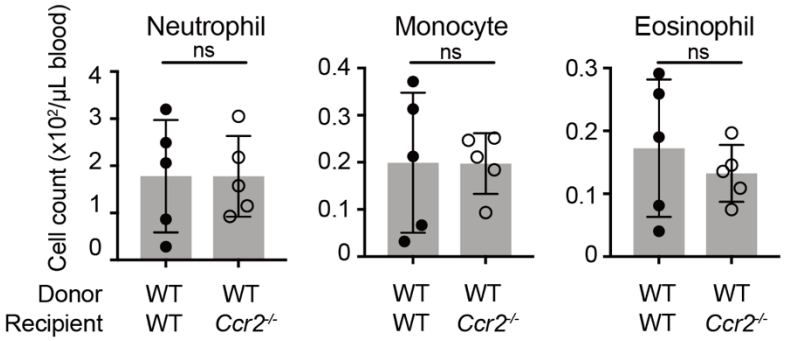

Supplementary Figure S4. CCR2 deficiency in radioresistant cells did not affect the numbers of neutrophils, monocytes, and eosinophils in the peripheral blood.

Lethally irradiated WT (n = 5) or *Ccr2*$^{-/-}$ (n = 5) mice were transplanted with WT BM cells. Twelve weeks later, BM-transplanted mice were treated topically with PBS and SDS on the right and left ears, respectively, for 6 consecutive days. Cell numbers of the indicated subsets in the peripheral blood were examined on day 6. Data are shown as values (*symbols*) and means ± SDs (*bars*). ns, Not significant.

Supplementary Figure S5.
Shibuya et al.

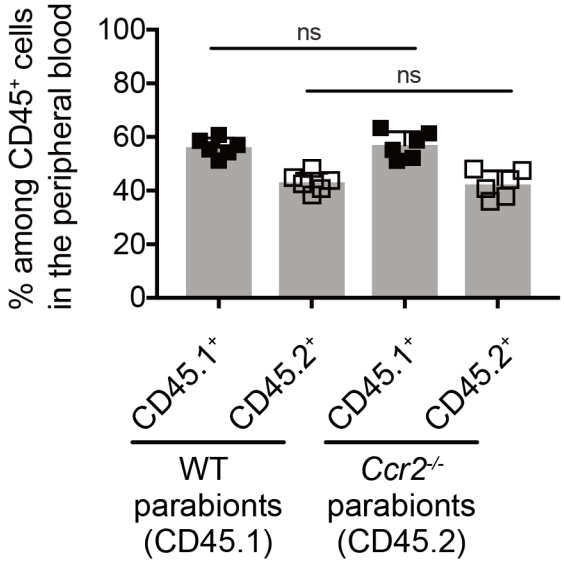

Supplementary Figure S5. Blood circulation was shared between the parabiont pairs.

Flow cytometric analysis of the composition of $CD45.1^+$ (WT-derived) and $CD45.2^+$ (*Ccr2*$^{-/-}$-derived) cells among $CD45^+$ cells in the peripheral blood from parabionts (n = 6) 2 weeks after surgical pairing. Data are shown as values (*symbols*) and means ± SDs (*bars*). ns, Not significant.

Supplementary Figure S6.
Shibuya et al.

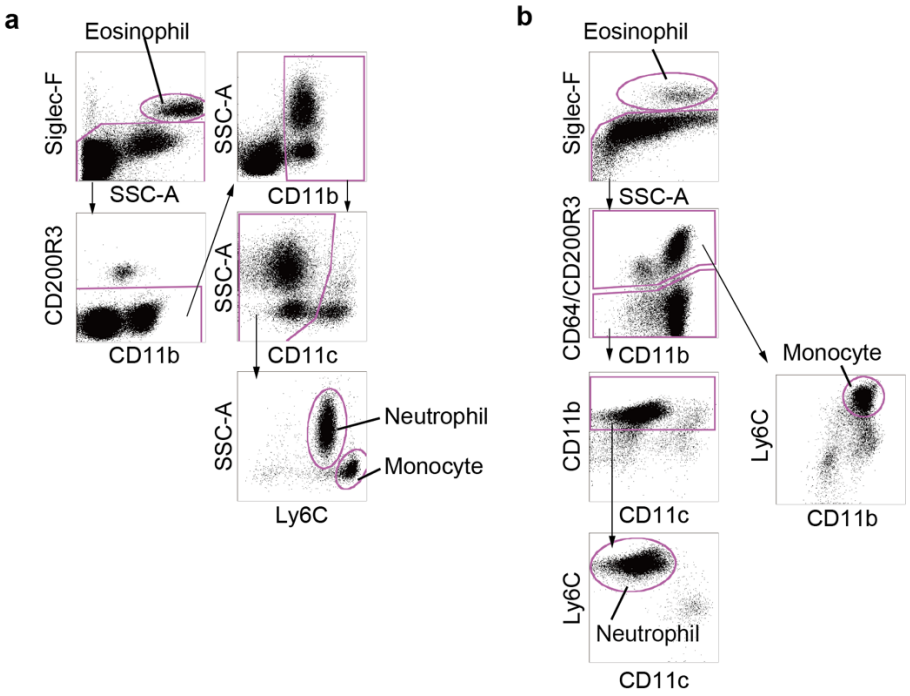

Supplementary Figure S6. Gating strategy for neutrophils, monocytes, and eosinophils.

WT mice (n = 5) were treated topically with PBS and SDS on the right and left ears, respectively, for 6 consecutive days, with the intraperitoneal injection of isotype rat IgG2a, followed by intraperitoneal injection of anti-rat IgG2a Ab on d-1, d1, d3, and d5. Flow cytometric analysis was performed on day 6. (**a**) Representative flow cytometry plots show the gating strategy for the following subsets from peripheral blood leukocytes: neutrophils (Siglec-F^{-}, CD200R3^{-}, CD11b^{+}, CD11c^{-}, Ly6C^{mid}), monocytes (Siglec-F^{-}, CD200R3^{-}, CD11b^{+}, CD11c^{-}, Ly6C^{high}), and eosinophils (Siglec-F^{+}). (**b**) Representative flow cytometry plots show the gating strategy for the following subsets from CD45^{+} cells in SDS-treated skin: neutrophils (Siglec-F^{-}, CD64^{-}, CD200R3^{-}, CD11b^{+}, CD11c^{-}, Ly6C^{mid}), monocytes (Siglec-F^{-}, CD64/CD200R3^{+}, CD11b^{+}, Ly6C^{high}), and eosinophils (Siglec-F^{+}).

Supplementary Figure S7.

Shibuya et al.

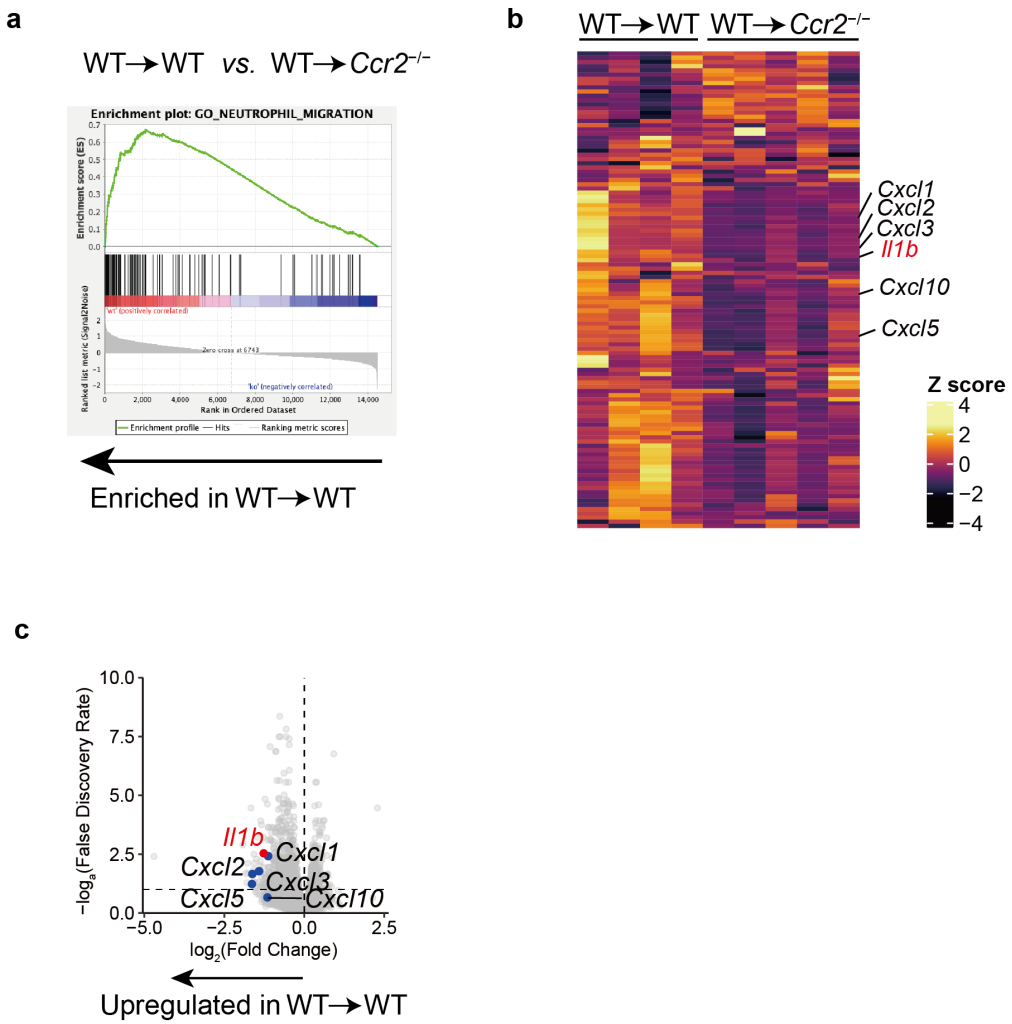

Supplementary Figure S7. CCR2 deficiency in radioresistant cells led to the downregulation of *Il1b* expression in SDS-treated skin.

Analyses of RNA-seq data obtained from SDS-treated skin of WT mice reconstituted with WT BM (n = 4) and *Ccr2*$^{-/-}$ mice reconstituted with WT BM (n = 5). Gene set enrichment analysis (**a**) and a heat map (**b**) of the GO_NEUTROPHIL_MIGRATION gene set (GO:1990266). (**c**) Volcano plots comparing gene expression between these two chimera groups.

Supplementary Figure S8.

Shibuya et al.

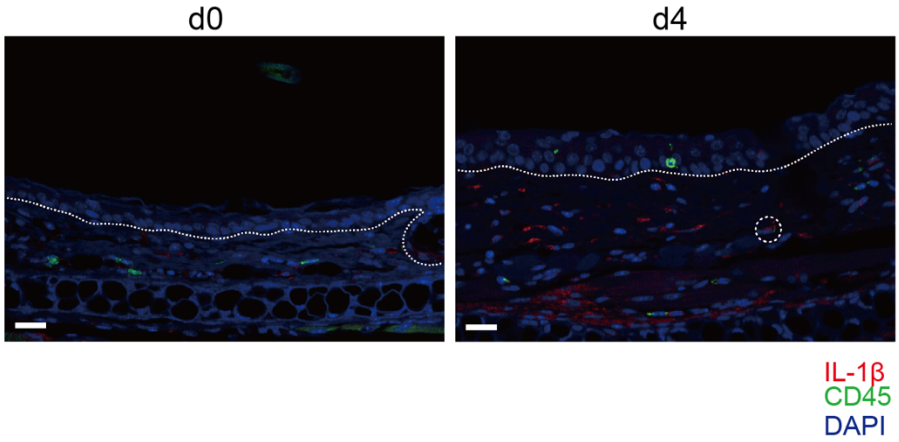

Supplementary Figure S8. Most IL-1β-expressing cells in SDS-treated skin were negative for CD45.

Expressions of IL-1β and CD45 protein in non-treated (d0) and SDS-treated (d4) ear skin were examined by immunofluorescence. Representative images are shown. Scale bars = 20 μm. DAPI, 4',6-diamidino-2-phenylindole. White circles indicate IL-1β/CD45-double positive cells.

Supplementary Figure S9.
Shibuya et al.

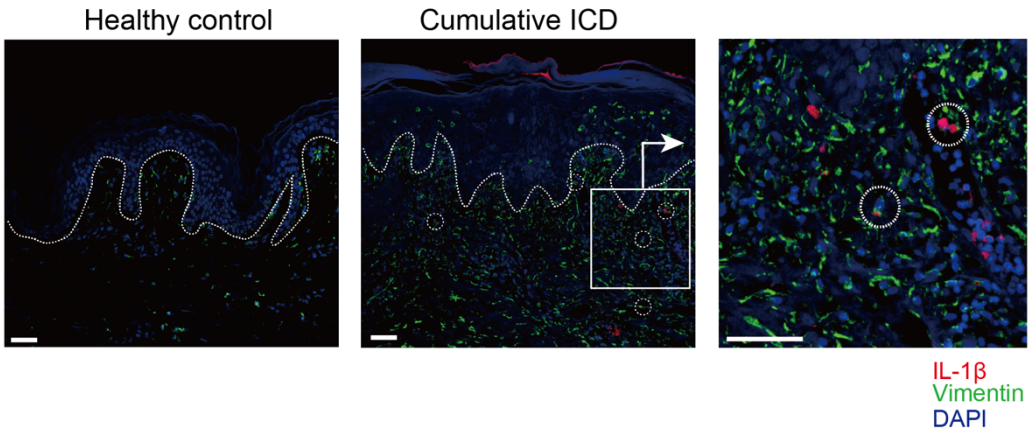

Supplementary Figure S9. Vimentin-positive cells were detected among IL-1β-expressing cells in lesional skin of human cumulative ICD.

Expression of IL-1β and vimentin protein in lesional skin of a patient with cumulative ICD and site-matched skin of a healthy subject were examined by immunofluorescence. Representative images are shown. Scale bars = 50 μm. DAPI, 4',6-diamidino-2-phenylindole. White circles indicate IL-1β/vimentin-double positive cells.

Supplementary Figure S10.
Shibuya et al.

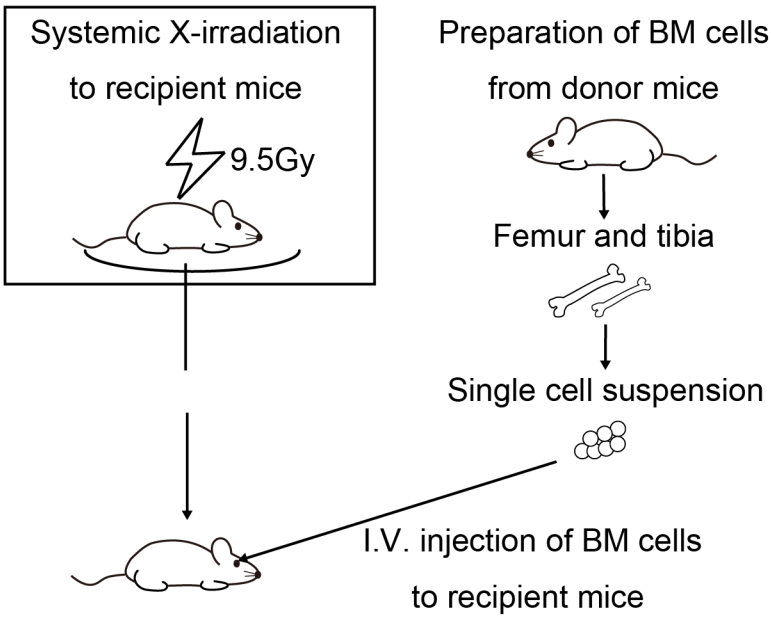

Supplementary Figure S10. Illustrations of the experimental steps for bone marrow transplantation.

Recipient mice were whole-body lethally X-irradiated (9.5 Gy) in an X-irradiator. BM cells were collected from femur and tibia of donor mice. Recipient mice received BM cells (3 x 10^6 cells) via the retro-orbital vein 3 h after irradiation.

Supplementary Figure S11.
Shibuya et al.

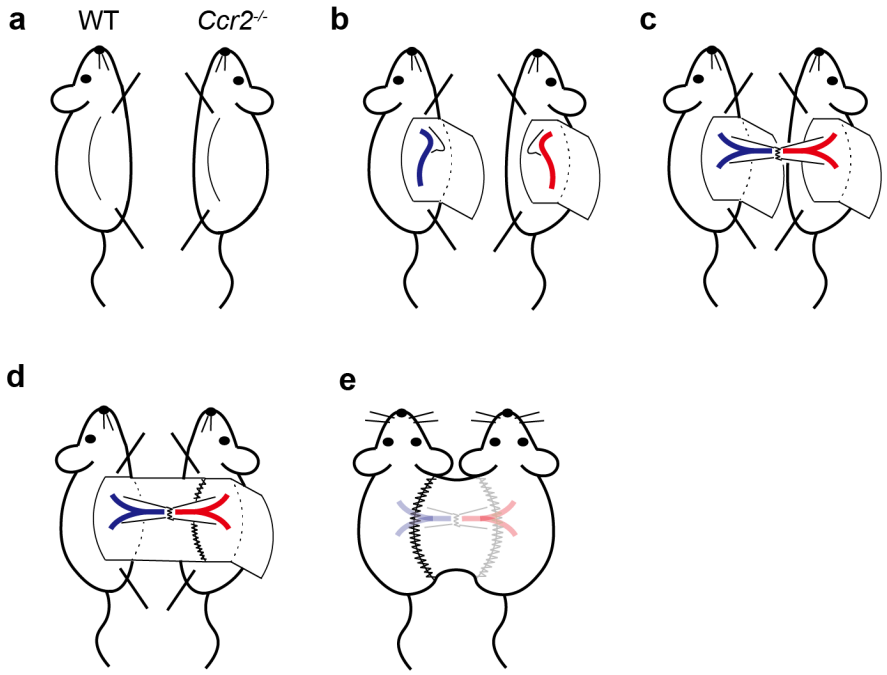

Supplementary Figure S11. Illustrations of procedures for parabiosis.

(a) Incision lines were designed on the right and left flank of WT and *Ccr2*$^{-/-}$ mice, respectively. **(b)** The skin was incised along the line using forceps and scissors to dissect skin and fat tissue from underlying muscles. Next, a muscle flap was dissected from the thoracic cage and the peritoneum. **(c)** Dissected muscle flaps from WT and *Ccr2*$^{-/-}$ mice are connected with each other by two sutures. **(d, e)** Ventral and dorsal skin flaps from the two mice are connected by sutures and wound clips to generate stable parabionts.

SUPPLEMENTARY MATERIALS AND METHODS

Animal experiments

All mice were maintained under specific pathogen-free conditions in the Institute of Laboratory Animals at Kyoto University Graduate School of Medicine. 7- to 10-week-old male mice were used for all the experiments. All experimental procedures were approved by the Institutional Animal Care and Use Committee of Kyoto University Graduate School of Medicine.

Antibodies

FITC anti-mouse I-A[b] (MHC class II) (AF6-120.1), FITC anti-CD45.2 (104), phycoerythrin (PE)-Siglec-F (E50-2440), allophycocyanin (APC) anti-Ly6G (1A8), biotin anti-CD117 (c-kit) (2B8), Brilliant Ultraviolet (BUV) 395 anti-CD45 (30-F11), and Brilliant Violet (BV) 605 anti-CD11b (M1/70) antibodies and BV605 streptavidin were purchased from BD Biosciences (San Jose, CA, USA). FITC anti-Ly6G (1A8), FITC anti-TCRβ (H57-597), PE-Cy7 anti-CD45.1 (A20), PE-Cy7 anti-CD11c (N418), APC anti-CD64 (X54-5/7.1), APC anti-CD200R3 (Ba13), APC anti-γδTCR (GL3), and Pacific Blue anti-Ly6C (HK1.4) were purchased from BioLegend (San Diego, CA, USA). PE anti-CD3e (145-2C11) antibody was purchased from Thermo Fisher Scientific (Waltham, MA, USA). PE anti-CD207 (Langerin) (caa828H10) antibody was purchased from Miltenyi Biotec (Bergisch Gladbach, Germany).

Anesthesia

Mice were anesthetized by subcutaneous injection of 0.3 mg/kg medetomidine (ZENOAQ, Fukushima, Japan), 4.0 mg/kg midazolam (Astellas Pharma, Tokyo, Japan), and 5.0 mg/kg butorphanol (Meiji Seika Pharma, Tokyo, Japan).

Assessment of ICD

Ear thickness was measured every day. Ear swelling was determined by subtracting the thickness on day 0 from the values obtained on each day. Ear swelling values obtained on day 6 were used for statistical analyses. Assessments of phenotypic appearance, histology and TEWL as well as flow cytometric cell counting in the skin were performed on day 6.

Processing of murine skin samples

Murine ears were excised and cut bisymmetrically. One half was used for flow cytometric analysis. The other half was used for histological analysis or RNA isolation. All skin samples were collected 15 h after the final application of PBS or SDS. For obtaining samples for ELISA, murine ear samples were collected as 6-mm skin biopsy specimens.

Preparation of single-cell suspensions

Ear samples were separated into dorsal and ventral sheets and digested for 105 min at 37°C in 5% CO_2 in RPMI 1640 containing 10% FCS, 1% penicillin- streptomycin, 1% sodium pyruvate, 1% MEM NEAA (Thermo Fisher Scientific), 0.25 mg/mL Liberase TL (Roche, Basel, Switzerland), and 0.3 mg/mL DNase I (Sigma-Aldrich, St. Louis, MO, USA). Digested skin sheets were placed in a Medicon (BD Biosciences) and homogenized using a Medimachine (BD Biosciences) for 7 min. Homogenized cells were

filtered using a 40 μm cell strainer (BD Biosciences) to obtain single-cell suspensions. Blood samples were collected from the submandibular vein and immediately transferred to EDTA-treated tubes. After hemolysis, blood samples were resuspended in RPMI 1640 containing 10% FCS, 1% penicillin-streptomycin, 1% sodium pyruvate, 1% MEM NEAA. BM cells were obtained by flushing the femurs and tibias with cold sterile RPMI 1640 medium containing 2% FCS. Collected cells were filtered through a 40 μm cell strainer and hemolyzed to obtain single-cell suspensions.

Flow cytometry

Single-cell suspensions obtained from the skin, peripheral blood, or BM were stained with the fixable viability dye eFluor 780 (Thermo Fisher Scientific), according to the manufacturer's instructions, for exclusion of dead cells. Next, nonspecific antibody binding was blocked with an anti-CD16/32 antibody (BD Biosciences), and then cells were stained for surface antigens. After the surface staining, cells were fixed with Cytofix/Cytoperm solution (BD Biosciences). Samples were assessed with the BD LSRFortessa cell analyzer (BD Biosciences), and data were analyzed using FlowJo software (BD Biosciences). Cell numbers of each cell subset were evaluated by using Flow-Count Fluorospheres (Beckman Coulter, Brea, CA, USA) and presented as numbers per tissue after exclusion of doublet and dead cells.

Histology

For murine samples, PBS- or SDS-treated ear skin was fixed in 10% formalin neutral buffer solution (Wako, Osaka, Japan) at room temperature overnight and then embedded in paraffin. For human samples, healthy skin or lesional skin of cumulative ICD was fixed

in 10% formalin overnight and then embedded in paraffin. Five-μm-thick sections were prepared and subjected to staining. Hematoxylin and eosin–stained sections were imaged with a digital microscope (BIOREVO BZ-9000, Keyence, Osaka, Japan). The average epidermal thicknesses were calculated from the distances between the stratum corneum and the bottom of the basal layer on the dorsal side measured at 5 locations at equal intervals in each image using cellSens Standard software (Olympus, Tokyo, Japan).

RNA *in situ* hybridization

Formalin-fixed paraffin embedded samples were sliced with a thickness of 5 μm and processed for RNA *in situ* detection by using the RNAscope 2.5 HD Assay-RED kit (Advanced Cell Diagnostics, Newark, CA, USA), as previously described (Hanakawa et al., 2019). Probes used in this study were as follows: Mm-Ccl2 (NM_011333.3), Hs-CCL2 (NM_002982.3), and the negative control probe DapB (Advanced Cell Diagnostics). Images were captured with a Nikon A1 confocal microscope (Nikon, Tokyo, Japan). The captured images were processed with Imaris software (Bitplane, Zurich, Switzerland) and were shown in pseudocolors.

Immunofluorescence

Formalin-fixed paraffin embedded samples were sliced with a thickness of 5 μm. Sections were blocked with donkey serum (abcam, Cambridge, MA, USA) at 10 % dilution for 60 min at room temperature.

For staining human/mouse vimentin or mouse CD45 following RNA *in situ* hybridization (RNAscope) of *Ccl2*, sections were incubated with rabbit monoclonal anti-human/mouse Vimentin (EPR3776) antibody (1:400) (abcam) or goat monoclonal anti-

mouse CD45 (D3F8Q) antibody (1:100) (Cell signaling, Danvers, MA, USA) overnight at 4 °C. Samples were washed with PBS and incubated for 30 min with Alexa Fluor 488–labeled donkey anti-rabbit IgG antibody (1:300) (Thermo Fisher Scientific) or Alexa Fluor 594–labeled donkey anti-goat IgG antibody (1:300) (Thermo Fisher Scientific) and 4',6-diamidino-2- phenylindole dihydrochloride (1:400) (Sigma-Aldrich).

For staining both IL-1β and vimentin in human and murine samples, sections were incubated with goat polyclonal anti-mouse IL-1β antibody at 10 μg/mL (R&D Systems, Minneapolis, MN, USA) or polyclonal anti-human IL-1β antibody at 2 μg/mL (abcam), and rabbit monoclonal anti-human/mouse Vimentin antibody (abcam) for 120 min at room temperature. Samples were washed and incubated for 30 min at room temperature with Alexa Fluor 594–labeled donkey anti-goat IgG antibody (1:300) (Thermo Fisher Scientific) and Alexa Fluor 488–labeled donkey anti-rabbit IgG antibody (Thermo Fisher Scientific).

For staining both IL-1β and CD45 in murine samples, sections were incubated with goat polyclonal anti-mouse IL-1β antibody (R&D Systems) for 120 min at room temperature. Samples were washed and incubated for 30 min at room temperature with Alexa Fluor 594–labeled donkey anti-goat IgG antibody (Thermo Fisher Scientific). After washing, samples were incubated with goat monoclonal anti-mouse CD45 antibody (Cell signaling) for 120 min at room temperature. After washing, samples were incubated for 30 min at room temperature with Alexa Fluor 488–labeled donkey anti-goat IgG antibody (Thermo Fisher Scientific) and 4',6-diamidino-2-phenylindole dihydrochloride (Sigma-Aldrich).

Stained sections were embedded with EcoMount (Biocare Medical, Pacheco, CA, USA). Images were captured with a Nikon A1 confocal microscope (Nikon). The

captured images were processed with Imaris software (Bitplane) and were shown in pseudocolors.

ELISA

CCL2 protein levels in PBS- or SDS-treated murine skin samples were measured using a Mouse CCL2/JE/MCP-1 Quantikine ELISA Kit (R&D Systems, Minneapolis, MN, USA), according to the manufacturer's instructions. Skin samples were collected as 6-mm skin biopsy specimens and weighed. Samples were frozen with liquid nitrogen and homogenized in 400 μL of T-PER Tissue Protein Extraction Reagent (Thermo Fisher Scientific) containing Halt Protease Inhibitor Cocktail (Thermo Fisher Scientific). The concentrations of CCL2 in supernatants were measured and weight-adjusted.

TEWL measurement

TEWL on PBS- or SDS-treated skin was measured on day 6 using VAPO SCAN AS-VT100RS (ASCH JAPAN, Tokyo, Japan).

***In vivo* blocking of cytokines**

Anti-CCL2 Ab (2H5) and polyclonal IgG isotype control were purchased from Bio X Cell (West Lebanon, NH, USA). Anti-IL-1β Ab (B122) and purified IgG isotype control (HTK888) were purchased from BioLegend. In CCL2 blocking experiments, mice were injected intradermally with 20 μg of anti-CCL2 Ab in the right ears and polyclonal IgG isotype control in the left ears on days 0, 2, and 4 during the 6-day SDS application period. In IL-1β blocking experiments, mice were injected intradermally with 20 μg of anti-IL-

1β Ab in the right ears and isotype IgG in the left ears on days 0, 2, and 4 during the 6-day SDS application period.

In vivo neutrophil depletion

For neutrophil depletion, a previously described method was used, with modifications (Boivin et al., 2020). In detail, mice were injected intraperitoneally with 250 μg of anti-Ly6G Ab (1A8, Bio X Cell) or rat IgG2a kappa isotype control (2A3, Bio X Cell) and then 2 h later with 250 μg of anti-rat IgG2a Ab (RG7/1.30, Bio X Cell) on days -1, 1, 3, and 5 during the 6-day period of SDS or PBS application.

In vivo rescue experiments with IL-1β

WT or *Ccr2*$^{-/-}$ mice were treated topically with PBS on the right ears and SDS on the left ears for 6 consecutive days, with the intradermal injection of recombinant mouse IL-1β (Biolegend) (5 ng) or PBS on day 2.

Generation of BM chimeric mice

BM chimeric mice were generated as previously described (Otsuka et al., 2010). Experimental steps are illustrated in Supplementary Figure S10. Briefly, recipient mice were whole-body lethally X-irradiated (9.5 Gy) for BM transplantation in an X-irradiator MBR-1520R-4 (Hitachi Medical Corp., Tokyo, Japan). Recipient mice received BM cells (3 x 10^6 cells) via the retro-orbital vein 3 h after irradiation. BM cells were collected as described in “Preparation of single-cell suspensions”. The chimeric mice were used for the indicated experiment 12 weeks after transplantation.

Parabiosis

Pairs of parabiotic mice consisting of CD45.1^{+} WT and CD45.2^{+} *Ccr2*$^{-/-}$ mice were generated, as described previously (Conboy et al. 2013; Duyverman et al. 2012). Surgical procedures are illustrated in Supplementary Figure S11. Briefly, anesthetized WT and *Ccr2*$^{-/-}$ mice were shaved on the right and left flank, respectively. After marking the incision lines on the skin, we incised the skin along the line using forceps and scissors and dissected skin and fat tissue from underlying muscles. A muscle flap is dissected from the thoracic cage and the peritoneum. We connected these dissected muscle flaps with each other by two sutures and closed the skin with wound clips (MikRon Precision Inc., Gardena, CA). Topical application of SDS or PBS on the ears of parabionts was commenced 2 weeks after the surgical joining.

RNA isolation

Total RNA was extracted with TRIzol reagent (Invitrogen, Carlsbad, CA, USA) and purified with RNeasy mini kit (Qiagen, Hilden, Germany) according to the manufacturers' protocol.

Quantitative reverse transcription polymerase chain reaction (RT-PCR)

cDNA was reverse transcribed from total RNA samples by using Prime Script RT reagent kit (Takara Bio, Otsu, Japan). Quantitative RT-PCR was performed by monitoring the synthesis of double-stranded DNA during the various PCR cycles with SYBR Green I (Roche, Basel, Switzerland) and the LightCycler real-time PCR apparatus (Roche), according to the manufacturer's instructions. All primers were obtained from Greiner Japan (Tokyo, Japan). The primer sequences were as follows: *Gapdh*, 5'-AGG TCG GTG

TGA ACG GAT TTG-3' (forward) and 5'-GGG GTC GTT GAT GGC AAC A-3' (reverse); *Ccl2* 5'-TAA AAA CCT GGA TCG GAA CCA AA-3' (forward) and 5'-GCA TTA GCT TCA GAT TTA CGG GT-3' (reverse). The cycling conditions were as follows: initial enzyme activation at 95 °C for 10 min, followed by 45 cycles at 95 °C for 10 sec and 60 °C for 20 sec. Gene-specific fluorescence was measured at 60 °C. For each sample, duplicate test reactions were analyzed for gene expression, and results were normalized to those of the housekeeping *Gapdh* gene.

RNA sequencing

RNA-seq libraries were generated using NEBNext Ultra II RNA Library kit for Illumina (New England Biolabs, Ipswich, MA, USA) according to the manufacturer's protocol and sequenced on the HiSeq 2500 or 4000 platform (Illumina, San Diego, CA, USA). Sequenced reads were quantified using kallisto quant (version .0.44.0) (Bray et al., 2016) against the Mus musculus transcriptome (GRCm38.96). Differential expression analysis was conducted using Wald test implemented in the R package, Sleuth (version 0.30.0) (Pimentel et al., 2017). Differentially expressed genes were defined as those with adjusted P value < 0.05 and log2(fold change) > 1. Gene Set Enrichment Analysis (GSEA) was conducted using GSEA software (version 4.1.0) (Daly et al., 2003; Subramanian et al., 2005) with default parameters.

Statistical analysis

Unless otherwise indicated, results are presented as values (symbols) and means ± SDs and are representative of at least three independent experiments. Comparisons between two experimental groups were analyzed for statistical significance by Student's t-test. For

multiple pairwise comparisons, *P* values were adjusted using the Bonferroni correction. $P < 0.05$ were considered to be significantly different. Multiple comparisons to a single control group were analyzed for statistical significance by Dunnett's test.

REFERENCES

Boivin G, Faget J, Ancey PB, Gkasti A, Mussard J, Engblom C, et al. Durable and controlled depletion of neutrophils in mice. Nat Commun. 2020;11:1–9.

Bray NL, Pimentel H, Melsted P, Pachter L. Near-optimal probabilistic RNA-seq quantification. Nat Biotechnol. 2016;34:525–7.

Conboy MJ, Conboy IM, and Rando TA. Heterochronic parabiosis: historical perspective and methodological considerations for studies of aging and longevity. Aging Cell. 2013;12:525-30.

Daly MJ, Patterson N, Mesirov JP, Golub TR, Tamayo P, Spiegelman B. PGC-1α-responsive genes involved in oxidative phosphorylation are coordinately downregulated in human diabetes. Nat Genet. 2003;34:267–73.

Duyverman AMMJ, Kohno M, Duda DG, Jain RK, Fukumura D. A transient parabiosis skin transplantation model in mice. Nat Protoc. 2012;7:763–70.

Hanakawa S, Kitoh A, Shibuya R, Dainichi T, Nomura T, Honda T, et al. Percutaneous sensitization is limited by in situ inhibition of cutaneous dendritic cell migration through skin-resident regulatory T cells. J Allergy Clin Immunol. 2019;144:1343-1353.e8.

Otsuka K, Hirabayashi Y, Tsuboi I, and Inoue T. Regeneration capability of $Lin^{-/-}$ c-

$Kit^+/Sca\text{-}1^+$ cells with or without radiation exposure for repopulation of peripheral blood in lethally irradiated mice monitored using Ly5.1 isotype on days 35, 90, and 270 after transplantation. Exp Hematol. 2010;38;417–425.

Pimentel H, Bray NL, Puente S, Melsted P, Pachter L. Differential analysis of RNA-seq incorporating quantification uncertainty. Nat Methods. 2017;14:687–90.

Subramanian A, Tamayo P, Mootha VK, Mukherjee S, Ebert BL, Gillette MA, et al. Gene set enrichment analysis: A knowledge-based approach for interpreting genome-wide expression profiles. Proc Natl Acad Sci U S A. 2005;102:15545–50.